



# Role of silt and clay fractions in organic carbon and nitrogen stabilization in soils of some old fruit orchards in the Nile floodplain, Sohag Governorate, Egypt

Fatma N. Thabit<sup>1</sup> · Abdel-Hamid El-Shater<sup>2</sup> · Wafaa Soliman<sup>2</sup>

Received: 27 October 2022 / Accepted: 6 March 2023 / Published online: 21 March 2023  
© The Author(s) 2023

## Abstract

**Purpose** Study the effect of both silt and clay fractions on stabilizing organic carbon and total nitrogen in soils of some old cultivated fruit orchards in Sohag, Egypt.

**Methods** Eleven surface soil samples (0–15 cm) were collected. Silt (63–2  $\mu\text{m}$ ) and clay (< 2  $\mu\text{m}$ ) fractions were separated from soils and analyzed for cation exchange capacity (CEC), organic carbon (OC), total nitrogen (TN), specific surface area (SSA), X-ray diffraction (XRD) and Fourier Transform Infrared (FTIR) spectroscopic analysis were determined using the standard analysis methods.

**Results** The silt and clay were responsible for 77.49 to 93.34% of soil CEC. The SSA of clay was twice the silt, and the phyllosilicates (%) average was 29.83% and 62.70% in silt and clay. Other minerals, such as quartz, feldspar, and carbonate minerals, were detected in these fractions. The phyllosilicate species of clay were smectite-illite mixed layers (44.4–88.9%), Smectite (1.0–6.4% except one sample recorded 45.7%), Kaolinite (3.7–10.5%) and kaolinite/smectite mixed layers (2.0–8.2%). The average OC-silt and clay were 6.79 and 8.96 g OC kg<sup>-1</sup> soil (38.01 and 50.28% of soil OC). On average, the total nitrogen (TN) in silt and clay particles was 0.817 and 1.156 g N kg<sup>-1</sup> soil (35.88 and 50.66% of soil TN). The OC and N content significantly and positively correlated with CEC, SSA, and phyllosilicates in the fine fractions.

**Conclusion** Results showed that the soil's capacity to sequester OC and N is affected significantly by its fine particles' content, characteristics, and mineralogy.

**Keywords** Organic carbon · Total nitrogen · Clay · Silt · Carbon sequestration

## 1 Introduction

Climate, relief, land use, and human activities are some of the variables influencing soil organic matter (SOM) content. Soil fertility is significantly affected by the chemical, physical, and biological properties of the organic matter in the soil. Organic matter (OM) can increase soil permeability, erosion resistance, and water-holding capacity and regulate heat release and absorption in soil. Moreover, SOM provides plants with nutrients and improves soil fertility (Guo

et al. 2020). The cation exchange capacity (CEC) of soil organic matter varies between 150 and 300 cmol (+) kg<sup>-1</sup>, and its specific surface area is high (up to 800–900 m<sup>2</sup> g<sup>-1</sup>). Thus, the soil organic matter is responsible for a large part of soil surface CEC. Kumar et al. (2004) noticed a decrease in the CEC of soil fractions after removing the SOM with H<sub>2</sub>O<sub>2</sub>. The high specific surface and CEC of soil organic matter encourage the adsorption of plant macro- and micro-nutrients, organic substances like pesticides, and heavy metal cations (Sparks 2003; Johnston et al. 2009). Moreover, significant amounts of carbon are also present in soil organic matter, which serves as a source of energy for soil micro- and macroflora. Soil organic matter contributes significantly to the physiological functions of soil and soil colloid activity (Gurmu 2019). Increasing soil organic matter and organic carbon improves soil properties and quality as well as enhances the long-term sustainability of agriculture

✉ Fatma N. Thabit  
fatma.hamdoon@agr.sohag.edu.eg

<sup>1</sup> Soil and Water Department, Faculty of Agriculture, Sohag University, Sohag, Egypt

<sup>2</sup> Geology Department, Faculty of Science, Sohag University, Sohag, Egypt

and crop production (Blanco-Canqui et al. 2013; Prout et al. 2021; Guillaume et al. 2022).

Soil organic carbon (SOC) is the main component of soil organic matter. Since it is generally difficult to directly detect soil organic matter (SOM), soil organic carbon is used as a measure. So, it can be considered that SOC represents the amount of SOM. The total nitrogen content is one of the soil fertility indicators. Plants need nitrogen in large quantities, so nitrogen (N) is considered a limiting factor for plant growth. Mainly, nitrogen is derived from soil organic matter and the atmosphere (78% N), as this nutrient does not occur naturally in minerals or rocks (Poirier et al. 2020). Soil supplies plants with 50% to 80% of their requirements of N (Kundu and Ladha 1995). The majority of soil N is added through the addition of inorganic fertilizers and organic amendments (manure, green manure, and crop residues) to the soil, besides other sources such as precipitation, biological fixation, and gas adsorption (Wibowo and Kasno 2021).

Organic matter stabilization by the soil matrix is a function of the mineral fraction's chemical nature and its surfaces' capability to adsorb organic materials (Baldock and Skjemstad 2000). Clay minerals are significant components in sediments and soils, and they are frequently coated with natural organic matter to form organic–clay complexes in sedimentary and agricultural soil environments (Pan et al. 2010; Singh et al. 2018). The mechanisms of soil organic carbon (SOC) stabilization have received more attention because of their relationship with the global carbon cycle (Das et al. 2022). The SOC stabilization through the interaction with soil minerals slows the SOC breakdown, minimizes greenhouse gases ( $\text{CO}_2$  and  $\text{CH}_4$ ) emission from soils into the atmosphere and carbon sequestration in soil systems (Udom et al. 2015; Dhaliwal et al. 2020; Kleber et al. 2005). The specific surface area (SSA) of soil is the total surface area that can be found in a unit mass of soil, and it is closely related to other physical and chemical properties, such as cation exchange capacity, clay content, mineralogical composition, OM content, and porosity (Heister 2014). Due to the varied specific surface areas (SSAs) and surface charges of the various minerals in soils, the interaction between fine mineral particles and OM is probably influenced by the mineralogy of the soil (Churchman et al. 2020). Among the properties of soil, Wiesmeier et al. (2019) found that higher content of fine fractions (silt + clay) with a higher specific surface area might have favored SOC sorption to the soil mineral matrix. Hu et al. (2021) found that the soils dominated by 1:1 clay minerals (Kaolinite) showed reduced sequestration of organic carbon compared to soils dominated by 2:1 clay minerals (illite, montmorillonite, vermiculite). According to land use, Hassink and Whitmore (1997) found that the organic carbon content in forest and grassland soils was higher than in arable soils. Several ways exist for organic matter adsorption onto mineral phases

(Roychand et al. 2010) such as: (1) Organic cations may replace exchangeable cations on the surface of clay minerals, (2) Hydrogen bonding between polar functional groups on organic hydrophobic substances and mineral surfaces, (3) Intercalation of organic molecules between the layers of expanded clays such as montmorillonite. Also, polyvalent cations like  $\text{Ca}^{+2}$  are thought to act as bridges between negatively charged organic groups and negatively charged clay surfaces (Rowley et al. 2021; Das et al. 2022).

Furthermore, the saturated clay minerals with multivalent cations tend to stay flocculated, decreasing the mineralization of organic carbon adsorbed on their surfaces or escaping as globules between clay matrix packets. The organic compounds are enclosed in intergranular mesopores of clay particles and thus protect against the biological attack of decomposer organisms (Bock and Mayer 2000; Feng et al. 2013; Schlüter et al. 2022). Under very acidic conditions, Fe and Al oxides can stabilize SOM significantly (Heckman et al. 2018; Wei et al. 2021), and the sorptive capacity of these oxides is significantly reduced in near-neutral soil environments. Also, Fe and Al may form stable complexes with the dissolved organic matter in the acidic soils (Takahashi and Dahlgren 2016; Heckman et al. 2018).

Healthy soil is fundamental for producing crops used for feeding humans and livestock. SOC is a primary attribute in soil health assessment and generally correlates positively with crop yield. The accumulation of SOM through the association with mineral surfaces and the occlusion within soil particles produces organo-mineral complexes (OMC). The formation of OMC is commonly defined as SOC bound to fine fractions (silt and clay). Keeping this in view, this study was conducted to investigate the effect of characteristics and mineralogy of soil fine fractions on SOC storage in some soils located in the Nile floodplain. Although many studies have been done on the Nile's soils and sediments (for example, Faragallah and Essa 2006; Abu Seif and El-Shater 2010; Abu Seif 2015; El-Shater et al. 2020; Abu Seif et al. 2022), the point of SOC stabilization in these soils did not get its due attention. So, the main objectives of this study were: 1- characterization of silt and clay-sized fractions in soils collected from some old cultivated fruit orchards in the Nile floodplain, Sohag Governorate, Egypt; 2- determining the mineralogy of these two fractions and 3- investigating the role of these fractions in the stabilizing of organic C and total N in these soils.

## 2 Materials and Methods

### 2.1 Study area

The studied area included the soils of old fruit orchards located in the Nile floodplain, Sohag Governorate, Egypt. According

to US Soil Taxonomy (Soil Survey Staff 1996), these soils belong to the Entisols soil orders. They are usually sand, silt, and clay mixtures, different types of loams (Ghazala et al. 2018). Sohag Governorate extends between longitudes 31° 15' and 32° 15' E and latitudes 26° 00' and 27° 00' N (Supplementary material Fig. S1). The northern boundary of Sohag is Assiut governorate, and the southern boundary is Qena governorate, while it is surrounded from the east and west by the two Eocene limestone plateaus of western and eastern deserts with variable highs. The alluvial cultivated areas in Sohag governorate extend along the sides of the Nile stream. Climatologically, Sohag Governorate belongs to Egypt's arid belt (Omran 2008), where the summer is long, arid, and hot, the winter is short and warm, and the rainfall is rare. Generally, the hot season in Sohag lasts for five months, approximately from May to September; the average daily maximum temperature is above 35 °C. July is the hottest month of the year, with an average maximum of 39 °C and minimum of 26 °C. However, the winter season is about three months, starting from December to February, with a daily high temperature of an average of less than 25 °C. In Sohag, the coldest month is January, with an average high of 21° and low of 8 °C (<https://weatherspark.com/>).

## 2.2 Soil sampling and preparation

Eleven surface (0–15 cm) soil samples were collected from some fruit orchards located in the Nile floodplain of five districts (Al Balyana, Girga, Al Minshah, Akhmim, and Tima) in Sohag governorate (Supplementary material Table S1). The location map of Sohag governorate was produced using ArcGIS 10.4.1 software (ESRI 2016) showing the soil samples locations and including geographic (latitude/longitude) grids, scale bar, north arrow, and map key (Supplementary material Fig. S1). All these selected orchards were cultivated with different types of fruit trees, such as guava, mango, and citrus for (15–20) years except for those of Al Balyana and Girga were cultivated with banana trees. The irrigation water source for these orchards was the Nile River water. The collected soil samples were air dried at room temperature, all visible gravels, plant materials, leaves, and roots were removed, and then the soil samples were crushed using a wooden roller. Then, the soil samples were sieved through a 2 mm sieve. The sieved soil samples were mixed homogeneously and stored for different analyses. All the analyses of this study were done in the Laboratories of Soil and Water and Geology Departments, Faculties of Agriculture and Science, Sohag University, Sohag, Egypt.

## 2.3 Determination of physiochemical properties (pH, EC<sub>e</sub>, %CaCO<sub>3</sub>, texture, CEC, % OC and % TN) of bulk soil samples

Soil pH was measured in a soil-to-water (1:2.5) suspension using a pH meter with a glass electrode. The electrical conductivity of soil samples (EC<sub>e</sub>) was recorded in the soil paste extract with the conductivity meter (Jackson 1973). The calcimeter method was used to estimate the total calcium carbonate content (% CaCO<sub>3</sub>) in soil samples (Nelson 1982). The pipette method was used to determine the particle-size distribution of soil samples as described by Rowell (1994). The percentages of sand, silt, and clay fractions were calculated and plotted on the soil texture triangle diagram to determine the texture grades of these samples (Supplementary material Fig. S2).

The cation exchange capacity (CEC) of soil samples was measured using sodium acetate solution (1 M, pH = 8.2) for the saturation step and ammonium acetate solution (1 M, pH = 7) for the replacement step, then the replaced sodium ions were determined by using a flame photometer (Baruah and Barthakur 1997). Organic carbon (OC) (%) in soil samples was determined using the dichromate oxidation method, according to Nelson and Sommers (1996). Total nitrogen (TN) (%) was measured in soil samples using the microkjeldahl method (Jackson 1973).

## 2.4 Mineralogical analysis of soil fine fractions (silt and clay)

One hundred grams of each soil sample were treated with H<sub>2</sub>O<sub>2</sub> to remove the organic matter (Moore and Reynolds 1997), and the dithionite citrate-sodium bicarbonate method (Kunze and Dixon 1994) was used for removing of free iron oxides. Then the soil suspensions were dispersed using Na-hexametaphosphate and a vortex mixer for 15 min (Gee and Bauder 1994). The sand fraction was separated from soil suspensions through a 63- $\mu$ m sieve, and then each suspension was transferred into a sedimentation cylinder (1L) and stirred carefully using a plunger to achieve complete mixing. The silt (63–2  $\mu$ m) and clay (< 2  $\mu$ m) fractions were collected by siphoning from the suspension at the appropriate depth and time based on Stoke's law at room temperature and then centrifuged (Rowell 1994). The bulk samples of both silt and clay fractions were air-dried, ground in an agate mortar, and then investigated using X-ray diffraction (XRD). Origin (2018) software was used for drawing the XRD charts of the bulk samples of both silt and clay fractions (Figs. 1 and 2). The peak intensities of XRD were used for semi-quantitative estimation of these fractions' mineralogical composition (%) (Fig. 3).

Clay was orientated using the glass slide procedure to estimate the clay mineral species of clay fraction (Moore and

**Fig. 1** Representative X-ray diffractograms showing the bulk mineralogy of silt fractions in the studied soil samples (from sample 1 to sample 11)

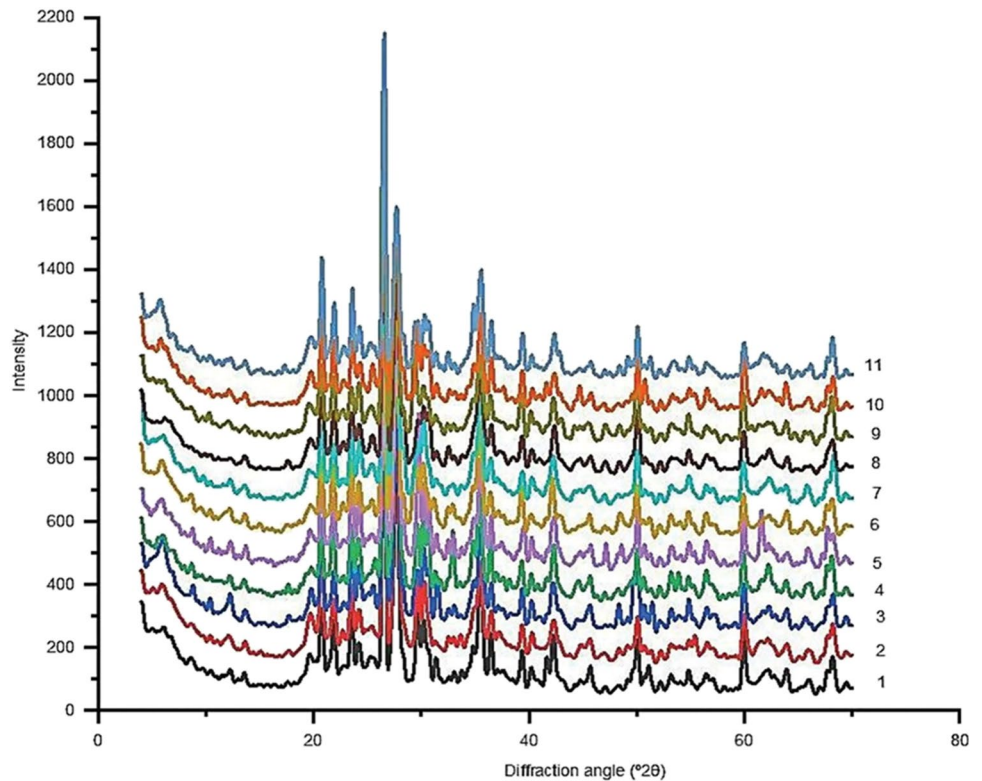
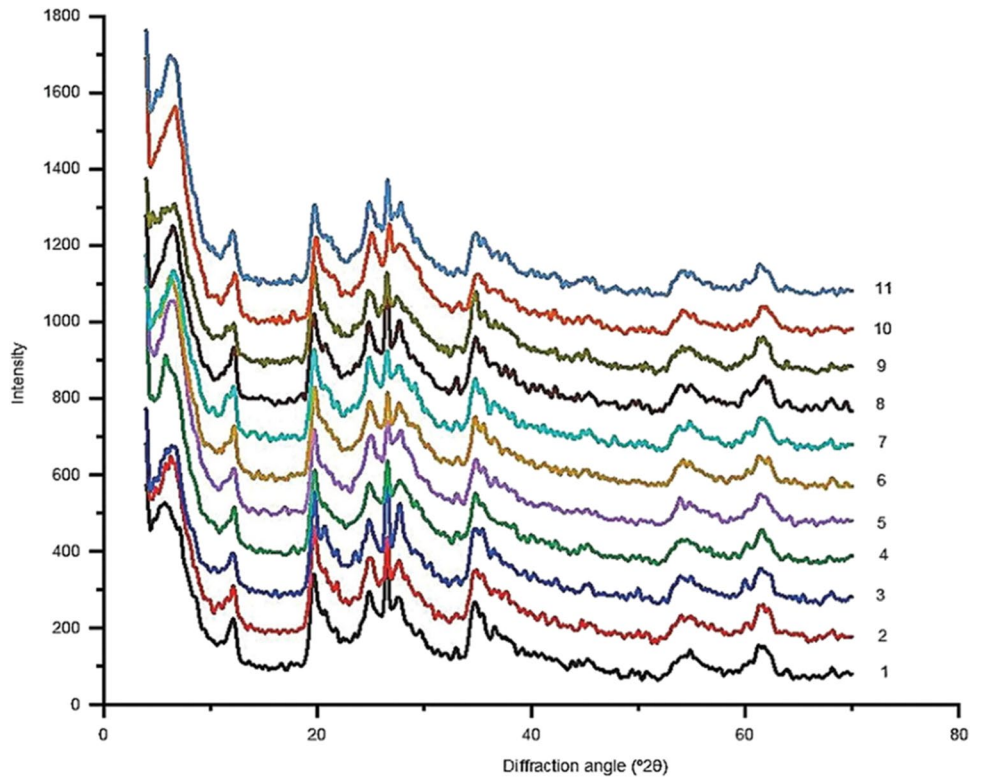


**Fig. 2** Representative X-ray diffractograms showing the bulk mineralogy of clay fractions in the studied soil samples (from sample 1 to sample 11)



Reynolds 1997). Samples of the clay fraction were saturated with K and Mg and then subjected to heating at a temperature of 550 °C (for the K slides), and ethylene glycolation

(for the Mg slides) processes (Al-Farraj 2008) and then were examined using X-ray diffraction (XRD). Philips X-ray diffraction equipment model PW/1710 with monochromatic,

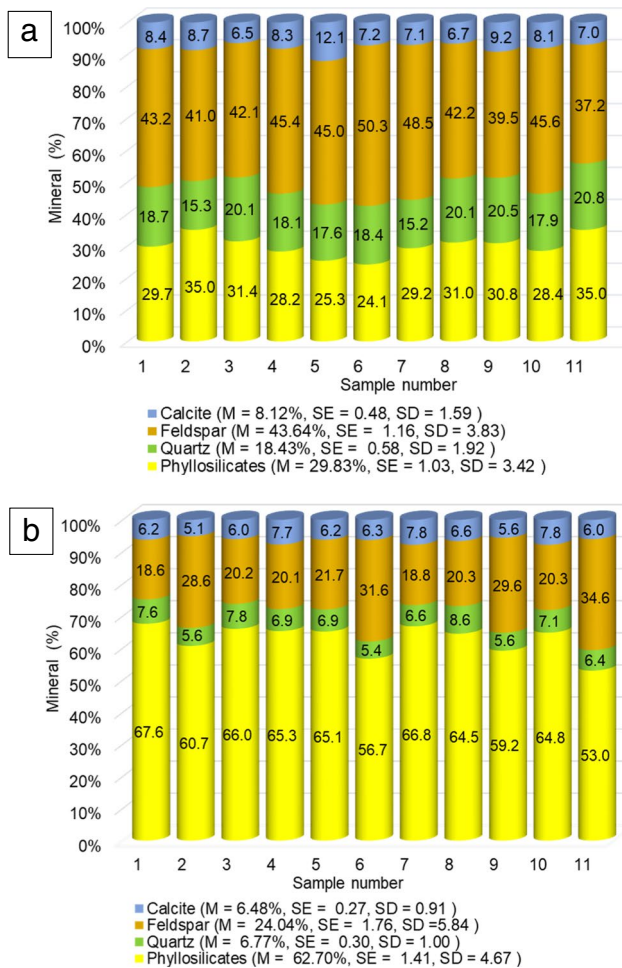


**Fig. 3** The bulk mineralogy of silt (a) and clay (b) fractions in the studied soil samples (from sample 1 to sample 11) (M=mean, SE=standard error of mean, SD=standard deviation)

Cu k - $\alpha$  ( $k = 1.54 \text{ \AA}$ ) radiation at 40 kV, 35 mA was used for all XRD investigations. The XRD data were processed numerically using the curve decomposition techniques described in Lanson (1997) for identification of the minerals species of clay fraction samples. This decomposition method involves fitting a computed curve to the recorded X-ray pattern corresponding to the sum of Gaussian or Lorentzian curves. The user decides initially how many curves (each curve corresponds to a clay mineral population) the program will have to cope with, and what are the approximate position, intensity, and width at half heights (WHH) of each curve. After selecting the initial parameters, the program fits the proposed curves with the measured pattern and exactly gives the values of position, intensity, and WHH. Every diffractogram was decomposed following the methods summarized by Moore and Reynolds (1997) and Barré et al. (2007) to estimate the illite and smectite proportions in each phase and determine each component's relative proportions using peak areas obtained by decomposition methods. The area

of every curve is proportional to the intensity multiplied by WHH. The curve's relative peak area is determined by dividing the peak area by the total of all the peak areas.

## 2.5 Separation of Fine fractions (Silt and Clay) for analysis

Fine fractions (silt and clay) were separated from bulk soil samples by mechanical dispersion in distilled water and sedimentation without chemical pretreatments. 500 ml of distilled water was added to 100 g of air-dried soil sample and left overnight. Then the suspensions were mixed with a vortex mixer for 15 min. The soil suspension was quantitatively transferred through a sieve (63  $\mu\text{m}$ ) into a 1 L sedimentation cylinder to separate the sand particles above the sieve. Then the silt (63–2  $\mu\text{m}$ ) and clay (<2  $\mu\text{m}$ ) fractions were separated from the cylinders following Stoke's law as the procedure mentioned above (Jackson 1979). Siphonation and centrifugation were repeated until enough silt and clay fractions were obtained.

## 2.6 Analysis of the separated fine fractions (silt and clay)

The separated fine fractions (silt and clay) were analyzed for different characteristics as follows:

### 2.6.1 Organic carbon (OC) and total nitrogen (TN) contents

Organic carbon (OC) (%) and total nitrogen (TN) (%) in each of the separated fine fractions (silt and clay) were determined using the dichromate oxidation method (Nelson and Sommers 1996) and micro-kjeldahl method (Jackson 1973), respectively.

### 2.6.2 Cation exchange capacity (CEC) of fine fractions (silt and clay)

The cation exchange capacity (CEC) of the separated fine fractions (silt and clay) was measured using the previously mentioned Baruah and Barthakur (1997) method.

### 2.6.3 The specific surface area (SSA) of fine fractions (silt and clay)

The specific surface area (SSA) of separated silt and clay fractions was determined from  $\text{N}_2$  gas adsorption–desorption isotherms at  $-196^\circ\text{C}$  using BELSORP max II equipment, Japan. The samples were initially outgassed at  $105^\circ\text{C}$  for 12 h under vacuum ( $10^{-4}$  Torr). BET surface area ( $S_{\text{BET}}$ ) was calculated by Brunauer -Emmett-Teller (BET) equation (Brunauer et al. 1938). Also, the total pore volume was obtained using a single point method at  $p/p_0 = 0.993$ , and the

mean pore volume was estimated using Barret-Joyner-Halenda (BJH) method.

#### 2.6.4 Fourier Transform Infrared (FTIR) spectroscopic analysis

Fourier Transform Infrared (FTIR) spectroscopic analysis of the separated silt and clay fractions was collected with a Bruker Alpha Platinum-ATR FTIR spectrometer using KBr pellets in the 4000–400  $\text{cm}^{-1}$  wave number region with a resolution of 4  $\text{cm}^{-1}$ . FTIR charts were drawn by using Origin (2018) software (Fig. 4).

### 2.7 Statistical analysis

The descriptive statistical analysis parameters (Mean, Standard error of mean (SE), Standard deviation (SD), Coefficient of variance (CV), Skewness, and Kurtosis) of data were done using SPSS version 22.0 software (IBM Corp. Released 2013). Also, the Pearson correlation coefficient analysis in SPSS version 22.0 software was used to do a bivariate correlation analysis between fine fractions (silt and clay) characteristics. The linear regression techniques in SAS software (SAS ver. 9.0, SAS Institute 2002) were used to analyze (1) the relationships between organic C content and total N content versus the fine fractions content (silt + clay %) in bulk soil, (2) the relationships between organic C and total N associated with silt fraction versus the silt content (%) in bulk soil, and (3) the relationships between C and N associated with clay fraction versus clay content (%) in bulk soil.

## 3 Results

### 3.1 The physiochemical properties of bulk soil samples

#### 3.1.1 Soil pH

The pH values indicate that the studied soils are slightly alkaline, with an average pH value fluctuating around 8 (Table 1). Generally, the pH values do not vary significantly throughout the studied soils, with some exceptions, such as those of Tima and Al Minshah districts (samples 6, 11) which exceed 8 (Table 1).

#### 3.1.2 Soil electrical conductivity ( $\text{EC}_e$ )

Electrical conductivity ( $\text{EC}_e$ ) values of the studied soil samples ranged between 0.90 and 2.71  $\text{dS m}^{-1}$ , with an average value of 1.59  $\text{dS m}^{-1}$  (Table 1).

### 3.1.3 Total calcium carbonate content (% $\text{CaCO}_3$ ) of soil samples

The total calcium carbonate percentage of the studied soils varied from 3.06 to 7.62% (Table 1).

#### 3.1.4 Soil texture

The data presented in Table 1 show that the clay (average, 41.61%) and silt (average, 38.69%) fractions are the major part of the studied soils with subordinate amounts of sand (average, 19.71%). Based on the soil texture triangle (Supplementary material Fig. S2), it is clear that the texture grades of the studied soil samples were classified into sandy clay loam, silty clay, silty clay loam, clay loam, and clay grades.

#### 3.1.5 Soil CEC

The CEC values of the studied bulk soil samples ranged from 31.26 to 56.83  $\text{cmol}(+) \text{kg}^{-1}$  with an average of 43.02  $\text{cmol}(+) \text{kg}^{-1}$  (Table 1).

#### 3.1.6 Soil organic carbon (OC) and total nitrogen (TN) contents

As shown in Table 1, the bulk soil OC contents ranged from 14.02 to 20.39  $\text{g OC Kg}^{-1}$  soil with an average of 17.76  $\text{g OC kg}^{-1}$ . However, the total N content in bulk soil samples ranged from 1.649 to 2.604  $\text{g N kg}^{-1}$  soil with an average of 2.280  $\text{g N kg}^{-1}$  soil (Table 1).

### 3.2 X-ray diffraction (XRD) analysis of fine fractions

#### 3.2.1 Bulk mineralogy of silt and clay fractions

The XRD patterns of the silt fractions of the studied soils show that the mineral content of these fractions is almost the same for all the studied soil samples. From XRD patterns, the silt fractions of these soils are mainly composed of feldspars (37.2–50.3%, with an average of 43.64%) and phyllosilicates (24.1 to 35.0%, with an average of 29.83%) with remarkable amounts of quartz (15.2–20.8%, with an average of 18.43%) and calcite (6.5–12.1% with an average of 8.12%) (Figs. 1, 3). The bulk mineralogy of clay fractions, according to their XRD patterns, is composed of 53.0–67.6% phyllosilicates with an average of 62.7%, feldspars (18.6–34.6% with an average value of 24.04%), in addition to small amounts of quartz and calcite (Figs. 2, 3).

**Fig. 4** FTIR spectra of silt (a) and clay (b) fractions in the studied soil samples (from sample 1 to sample 11)

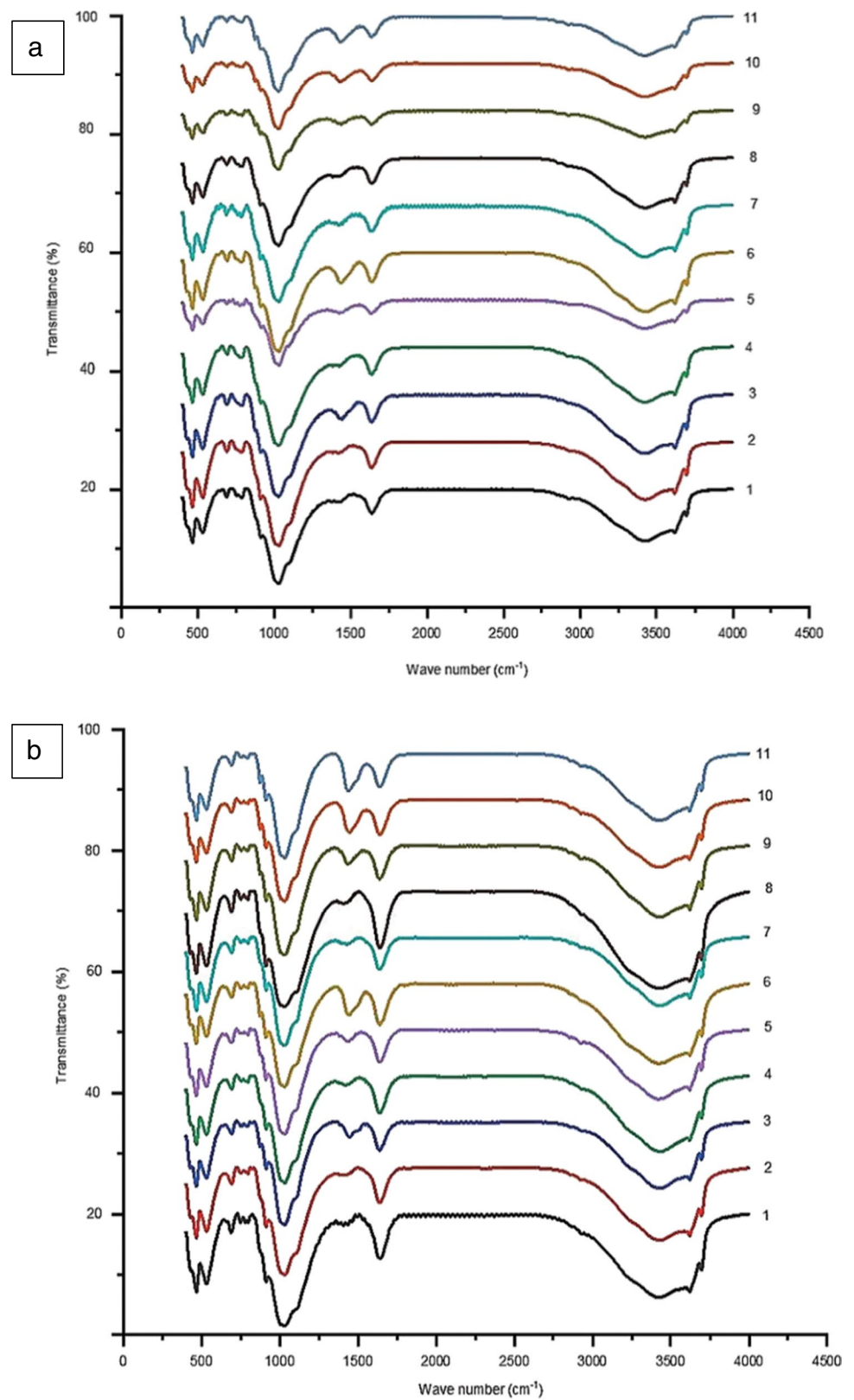


**Table 1** The physiochemical properties of bulk soil samples

Sample No	pH (1:2.5)	*EC <sub>e</sub> (dS m <sup>-1</sup> )	Total CaCO <sub>3</sub> (%)	Sand	Silt	Clay	Soil texture grade	*Soil CEC (cmol(+) Kg <sup>-1</sup> soil)	*Soil OC (g kg <sup>-1</sup> soil)	*Soil TN (g kg <sup>-1</sup> soil)
1	7.86	1.08	5.36	10.47	40.64	48.87	silty clay	43.00	19.11	2.474
2	7.80	1.04	5.08	5.38	39.00	55.61	clay	52.61	20.39	2.604
3	7.97	2.71	7.62	7.13	21.09	71.81	clay	56.83	18.26	2.517
4	7.82	1.04	4.47	10.82	51.71	37.49	silty clay loam	42.17	17.41	2.387
5	7.73	1.23	5.38	27.72	38.24	34.03	clay loam	43.74	16.56	1.953
6	8.17	2.36	4.63	8.59	37.67	53.72	clay	50.43	17.84	2.213
7	7.67	0.90	6.42	10.40	49.22	40.41	silty clay	39.91	19.11	2.474
8	7.78	2.51	6.26	11.90	46.21	41.93	silty clay	38.48	19.54	2.300
9	7.68	1.84	5.37	13.21	56.75	30.05	silty clay loam	42.52	18.69	2.561
10	7.92	1.08	3.06	56.48	21.49	22.07	sandy clay loam	31.26	14.02	1.649
11	8.20	1.72	3.81	54.71	23.52	21.73	sandy clay loam	32.22	14.44	1.953
Mean	7.87	1.59	5.22	19.71	38.69	41.61	-	43.02	17.76	2.280
*SE	0.05	0.20	0.38	5.63	3.70	4.57	-	2.38	0.61	0.093
*SD	0.18	0.67	1.26	18.66	12.26	15.15	-	7.90	2.04	0.307
*CV	2.28	42.16	24.15	94.68	31.70	36.40	-	18.37	11.46	13.47
Skewness	0.90	0.67	0.18	1.58	-0.29	0.53	-	0.23	-0.89	-1.00
Kurtosis	-0.12	-1.28	0.35	1.04	-1.03	0.08	-	-0.35	-0.06	0.06

\*EC<sub>e</sub> = the electrical conductivity of soil paste extract, \*CEC = cation exchange capacity

\*OC = organic carbon, \*TN = total nitrogen, \*SE = standard error of mean

\*SD = standard deviation, \*CV = coefficient of variance (CV = standard deviation × 100/ mean)

### 3.2.2 Clay mineral species of clay fractions

#### Qualitative analysis of the clay mineral species of clay fractions

The X-ray diffractograms of the analyzed soils' clay fractions reveal that the clay minerals differ remarkably from one soil to another (Table 2). Regarding the qualitative identification methods suggested by Brindley (1981), Velde (1995), Moore and Reynolds (1997), and Hillier (2003) and the curve decomposition procedure of Lanson (1997) and mentioned in El-Shater (2013), the minerals reflections behavior under conditions (air-dried, ethylene glycolation and heating to 550 °C) defined a group of clay minerals included by Smectite (Ca- montmorillonite), rich-smectite (smectite/illite mixed-layers) (S/I<sub>sm</sub>), rich-illite (illite/smectite mixed-layers) (S/I<sub>il</sub>), poorly crystallized illite (PCI), well-crystallized illite (WCI), kaolinite, and kaolinite/smectite (K/S) mixed layers.

#### Quantitative analysis of the clay mineral species of clay fractions

The rich-smectite (smectite /illite mixed-layers) (S/I<sub>sm</sub>) was the major clay mineral. It varied from 41.00 to 88.90% in the clay fractions of the investigated soils except one sample from Girga district (sample 4) recorded 1.20% S/I<sub>sm</sub> in its clay fraction. As for rich-illite (illite/smectite mixed-layers) (S/I<sub>il</sub>), it was found only in the orchard soils of the southern districts (Al Balyana, samples 1, and 2 and

Girga, samples 3 and 4), with values ranging between 9.20 and 43.20%. On the other hand, the Smectite (Ca- montmorillonite) showed a different behavior; where it was recorded in high values only in the orchard soils of the Girga district, sample 4 (45.70%). It completely disappeared from the orchard soils of Al Balyana (sample 1), Girga (sample 5), Al Minshah (sample 7), and Tima (samples 10 and 11), and it appeared again in small quantities (1.00–6.40%) in each of Al Balyana (sample 2) and Girga (sample 3), Al Minshah (sample 6) and Akhmim (samples 8, 9) districts. The poorly crystallized illite (PCI) was recorded in all the studied soils with a minor amount (2.10–10.70%) except for those of Girga, Akhmim, and Tima (sample 11). The well-crystallized illite (WCI) was traced in Tima district (sample 10) only. The kaolinite and kaolinite/smectite (K/S) are found in small amounts (3.70–10.50% and 2.00–8.20%, respectively) in all the studied soils.

### 3.3 Organic carbon (OC) content of fine fractions

The organic carbon (OC) content data of the separated silt and clay fractions are presented in Table 3. The concentration of OC associated with fine fractions ranged from 13.37 to 22.98 g C kg<sup>-1</sup> fraction for silt and from 18.39 to 30.92 g C kg<sup>-1</sup> fraction for clay with the averaged values 17.82 and 22.45 g C kg<sup>-1</sup> fraction, respectively (Table 3). The OC



**Table 2** The clay mineral species (%) of the clay fractions in the studied soil samples

Sample No	Phyllosilicates species (%) of clay fractions						
	Smectite (SM)	Mixed-layers (smectite/ illite)		Illite		Kaolinite (K)	Mixed-layers (kaolinite/ smectite) (K/S)
		*S/I <sub>sm</sub>	*I/S <sub>il</sub>	*PCI	*WCI		
1	-	41.00	39.90	3.50	-	9.20	6.40
2	4.50	53.40	26.10	2.10	-	10.50	3.40
3	6.40	71.00	9.20	-	-	5.80	7.60
4	45.70	1.20	43.20	-	-	4.10	5.80
5	-	87.90	-	1.60	-	7.10	3.40
6	2.10	79.90	-	6.20	-	6.50	5.30
7	-	77.90	-	7.80	-	6.10	8.20
8	1.00	74.80	-	10.40	-	8.00	5.80
9	4.40	88.00	-	-	-	3.70	3.90
10	-	88.90	-	-	2.20	4.60	4.30
11	-	83.40	-	5.10	-	9.50	2.00
Mean	*nd	67.95	nd	nd	nd	6.83	5.10
*SE	nd	8.07	nd	nd	nd	0.68	0.57
*SD	nd	26.78	nd	nd	nd	2.27	1.90
*CV	nd	39.41	nd	nd	nd	33.27	37.22
Skewness	nd	-1.83	nd	nd	nd	0.21	0.12
Kurtosis	nd	3.33	nd	nd	nd	-1.11	-0.69

\*I/S<sub>sm</sub> = rich-smectite (smectite /illite mixed-layers) mineral

\*I/S<sub>il</sub> = rich-illite (illite/ smectite mixed-layers) mineral, \*PCI = poorly crystallized illite

\*WCI = well crystallized illite. \*SE = standard error of mean, \*SD = standard deviation

\*CV = coefficient of variance (CV = standard deviation × 100/ mean)

\*nd = Not detected (due to the absence of some minerals from the samples, which are symbolized by dashes)

concentration (g OC kg<sup>-1</sup> fraction) in each fraction (silt or clay) was multiplied by this fraction's corresponding dry mass to calculate the expression of g OC kg<sup>-1</sup> soil for each fraction (Matus et al. 2016) (Table 3). The OC concentration associated with fine fractions on a bulk soil basis ranged from 3.17 to 10.20 g OC kg<sup>-1</sup> soil for silt and from 5.53 to 13.80 g OC kg<sup>-1</sup> soil for clay fraction with averaged values 6.79, 8.96 g OC kg<sup>-1</sup> soil, respectively. As regards the proportion of OC in fine fractions relative to OC in bulk soils, results in Table 3 showed that 17.37–54.57% of bulk soil OC content was associated with silt fraction with an average of 38.01%, while the OC-associated with clay fraction was 29.57–75.58% of bulk soils OC with an average of 50.28%.

### 3.4 Total nitrogen (TN) content of fine fractions

Results in Table 3 illustrate the total nitrogen content of the separated fine fractions (silt and clay). The concentration of total N associated with silt and clay fractions ranged from 1.649 to 3.038 g N kg<sup>-1</sup> fraction and from 2.278 to 4.340 g N kg<sup>-1</sup> fraction with an average of 2.156 and 2.914 g N kg<sup>-1</sup> fraction, respectively. On bulk soil basis, the total N

associated with silt fraction ranged from 0.398 to 1.293 g N kg<sup>-1</sup> soil with an average of 0.817 g N kg<sup>-1</sup> soil; however, the total N associated with clay fraction ranged from 0.685 to 1.776 g N kg<sup>-1</sup> soil with an average of 1.156 g N kg<sup>-1</sup> soil. On average, 35.88 and 50.66% of total nitrogen in bulk soil are associated with silt and clay fractions, respectively (Table 3).

### 3.5 Cation Exchange Capacity (CEC) of fine fractions

Results in Table 4 illustrated that the CEC values of silt fractions irregularly fluctuated from 26.35 to 46.61 cmol(+) kg<sup>-1</sup> with an average of 34.58 cmol(+) kg<sup>-1</sup> fraction. The clay fractions recorded CEC values varied from 51.48 to 72.52 cmol(+) kg<sup>-1</sup> fraction, averaging 61.59 cmol(+) kg<sup>-1</sup> fraction. Results in Table 4 showed that the fine fractions (silt and clay) made the largest contributions to the soil CEC and were collectively responsible for 77.49 to 93.34% of the total soil CEC (calculated depending on every fraction's CEC and its percentage in the bulk soil samples) with an average of 87.82%. Separately, the contribution of silt fraction alone to the total soil CEC ranged from 12.29 to

**Table 3** Organic C content ( $\text{g OC kg}^{-1}$ ) and total nitrogen (TN) content ( $\text{g N kg}^{-1}$ ) of fine fractions

Sample No	OC- concentration (fine fractions basis)		*OC- concentration (bulk soil basis)		Proportion of OC in fractions relative to OC in bulk soil		TN- concentration (fine fractions basis)		*TN- concentration (bulk soil basis)		Proportion of TN in fractions relative to TN in bulk soil	
	Silt ( $63\text{--}2\ \mu\text{m}$ )	Clay ( $<2\ \mu\text{m}$ )	Silt ( $63\text{--}2\ \mu\text{m}$ )	Clay ( $<2\ \mu\text{m}$ )	Silt ( $63\text{--}2\ \mu\text{m}$ )	Clay ( $<2\ \mu\text{m}$ )	Silt ( $63\text{--}2\ \mu\text{m}$ )	Clay ( $<2\ \mu\text{m}$ )	Silt ( $63\text{--}2\ \mu\text{m}$ )	Clay ( $<2\ \mu\text{m}$ )	Silt ( $63\text{--}2\ \mu\text{m}$ )	Clay ( $<2\ \mu\text{m}$ )
1	17.97	20.89	7.30	10.21	38.21	53.42	2.148	3.038	0.873	1.485	35.29	60.02
2	17.13	21.73	6.68	12.08	32.77	59.27	1.953	2.604	0.762	1.448	29.25	55.61
3	15.04	19.22	3.17	13.80	17.37	75.58	1.888	2.474	0.398	1.776	15.82	70.57
4	13.37	21.31	6.91	7.99	39.71	45.88	1.649	3.038	0.853	1.139	35.73	47.72
5	15.46	26.74	5.91	9.10	35.69	54.95	2.083	2.929	0.797	0.997	40.79	51.05
6	17.55	18.80	6.61	10.10	37.06	56.62	1.910	2.278	0.719	1.224	32.50	55.30
7	18.80	20.89	9.26	8.44	48.43	44.18	2.040	2.778	1.004	1.122	40.59	45.37
8	19.22	20.06	8.88	8.41	45.46	43.04	2.257	2.561	1.043	1.074	45.34	46.67
9	17.99	18.39	10.20	5.53	54.57	29.57	2.278	2.278	1.293	0.685	50.50	26.74
10	20.48	28.00	4.40	6.18	31.40	44.08	2.474	3.732	0.532	0.824	32.24	49.94
11	22.98	30.92	5.41	6.72	37.43	46.54	3.038	4.340	0.715	0.943	36.59	48.29
Mean	17.82	22.45	6.79	8.96	38.01	50.28	2.156	2.914	0.817	1.156	35.88	50.66
*SE	0.80	1.26	0.63	0.75	2.93	3.55	0.11	0.19	0.07	0.09	2.73	3.25
*SD	2.65	4.17	2.10	2.49	9.72	11.76	0.37	0.63	0.24	0.32	9.06	10.78
*CV	14.88	18.56	30.85	27.80	25.58	23.39	17.06	21.64	29.91	27.26	25.26	21.27
Skewness	0.25	1.16	-0.01	0.58	-0.42	0.56	1.34	1.36	0.24	0.56	-0.70	-0.49
Kurtosis	0.46	0.12	-0.36	-0.02	1.46	1.67	2.76	1.61	0.60	0.12	1.78	2.56

\*OC- concentration (bulk soil basis) (g OC  $\text{kg}^{-1}$  soil) = The OC concentration (g OC  $\text{kg}^{-1}$  fraction) in each fraction (silt or clay) x this fraction's corresponding dry mass\*TN- concentration (bulk soil basis) (g TN  $\text{kg}^{-1}$  soil) = The TN concentration (g TN  $\text{kg}^{-1}$  fraction) in each fraction (silt or clay) x this fraction's corresponding dry mass\*SE = standard error of mean, \*SD = standard deviation, \*CV = coefficient of variance (CV = standard deviation  $\times$  100/ mean)

**Table 4** Cation exchange capacity (CEC), specific surface area ( $S_{BET}$ ), total pore volume (TPV), and mean pore diameter (MPD) of fine fractions

Sample No	CEC of fine fractions (cmol(+) Kg <sup>-1</sup> fraction)		The contribution of silt fraction to the soil CEC (%)	The contribution of clay fraction to the soil CEC (%)	*The contribution of fine fractions to the soil CEC	$S_{BET}$ (m <sup>2</sup> g <sup>-1</sup> ) of fine fractions		TPV (cm <sup>3</sup> g <sup>-1</sup> ) of fine fractions		MPD (nm) of fine fractions	
	Silt (63-2 μm)	Clay (<2 μm)				Silt (63-2 μm)	Clay (<2 μm)	Silt (63-2 μm)	Clay (<2 μm)	Silt (63-2 μm)	Clay (<2 μm)
1	30.87	53.00	29.18	60.23	89.41	45.179	59.250	0.0844	0.1184	7.4713	7.9935
2	38.70	61.17	28.68	64.66	93.34	49.749	84.192	0.0867	0.1389	6.9702	5.8974
3	33.13	62.00	12.29	78.34	90.64	40.061	87.561	0.0807	0.1302	8.0550	5.3367
4	31.22	54.04	38.28	48.04	86.32	35.463	64.852	0.0736	0.1230	8.2966	7.5845
5	37.39	66.96	32.69	52.10	84.79	37.573	67.607	0.0747	0.1218	7.9467	7.2034
6	34.35	60.65	25.66	64.60	90.25	46.489	62.602	0.0812	0.1056	6.9909	6.7498
7	28.04	57.13	34.59	57.84	92.43	43.505	82.806	0.0783	0.1278	7.1956	6.1718
8	26.35	51.48	31.64	56.09	87.73	36.627	69.226	0.0718	0.1104	7.8400	6.3803
9	30.22	72.52	40.33	51.26	91.59	48.417	95.724	0.0863	0.1424	7.1307	5.9519
10	43.52	67.39	29.92	47.57	77.49	22.967	79.546	0.0590	0.1388	10.268	6.9780
11	46.61	71.17	34.03	48.01	82.04	34.792	70.954	0.0755	0.1355	8.6781	7.6404
Mean	34.58	61.59	30.66	57.16	87.82	40.075	74.938	0.0775	0.1266	7.8948	6.7171
*SE	1.92	2.19	2.24	2.84	1.46	2.340	3.519	0.0024	0.0036	0.2917	0.2543
*SD	6.37	7.26	7.43	9.44	4.84	7.760	11.672	0.0080	0.0120	0.9676	0.8434
*CV	18.43	11.80	24.24	16.51	5.51	19.363	15.576	10.294	9.5103	12.256	12.556
Skewness	0.72	0.11	-1.45	1.11	-1.05	-0.886	0.381	-1.128	-0.415	1.555	-0.036
Kurtosis	-0.30	-1.26	3.46	1.19	0.62	1.051	-0.987	1.893	-0.829	2.972	-1.075

\*The contribution of fine fractions to the soil CEC (%) = the contribution of silt fraction to the soil CEC (%) + the contribution of clay fraction to the soil CEC (%)

\*SE = standard error of mean, \*SD = standard deviation, \*CV = coefficient of variance (CV = standard deviation × 100/ mean)

40.33%, with an average of 30.66%. At the same time, the corresponding values of the clay fraction ranged between 47.57 and 78.34%, with an average of 57.16% (Table 4).

### 3.6 The specific surface area (SBET), total pore volume, and mean pore diameter of fine fractions

Data of the specific surface area ( $S_{\text{BET}}$ ), total pore volume (TPV), and mean pore diameter (MPD) of both silt and clay fractions of the studied soils are shown in Table 4. It is easily noticeable that silt fraction attains the lower surface area ( $S_{\text{BET}}$ ) (22.967–49.749  $\text{m}^2 \text{g}^{-1}$ ) and total pore volume (TPV) (0.0590–0.0867  $\text{cm}^3 \text{g}^{-1}$ ) values. On the other hand, clay fractions have the highest surface area ( $S_{\text{BET}}$ ) (59.25–95.72  $\text{m}^2 \text{g}^{-1}$ ) and total pore volume (TPV) (0.1056–0.1389  $\text{cm}^3 \text{g}^{-1}$ ) values. As for the mean pore diameter (MPD) values, they were larger in the silt fractions (6.9702–10.268 nm) compared to those in the clay fractions (5.3367–7.9935 nm).

### 3.7 Fourier Transform Infrared (FTIR) spectroscopy analysis of fine fractions

Fourier Transform Infrared (FTIR) spectroscopy analysis is a simple and rapid technique. The IR spectrum of clay minerals is sensitive to their chemical characteristics and composition, isomorphic substitutions, and structural variations. So, FTIR spectroscopy is the tool that provides background about the composition and structure of clay minerals, as well as their interactions with organic or inorganic compounds (Johnston 2010; Komadel 2003; Madejova 2003). The IR spectra of all silt and clay samples are nearly the same, with slight differences between the IR spectra of each of these two fractions (Fig. 4 and Table 5). From the IR spectra of these two fractions (silt and clay), it can be easy to track the clay mineral groups (smectite, kaolinite, and illite) and non-clay minerals (feldspars, quartz, and calcite) identified by XRD analysis, in addition to the presence of organic functional groups, as the following:

**Table 5** Main bands of FTIR spectrum of silt and clay fractions in the studied soil samples

Sample No	Band ( $\text{cm}^{-1}$ ) Silt (63–2 $\mu\text{m}$ )
1	(3696, 3620, 3423, 2924, 2854, 1640, 1546, 1408, 1380, 1031, 914, 786, 756, 693, 691, 533, 467)
2	(3696, 3621, 3424, 2929, 1638, 1418, 1384, 1031, 914, 794, 779, 534, 467)
3	(3697, 3621, 3425, 2929, 2855, 1639, 1444, 1032, 914, 876, 792, 764, 693, 632, 534, 467)
4	(3696, 3621, 3425, 2966, 2926, 2856, 1639, 1427, 1384, 1031, 914, 780, 535, 467)
5	(3697, 3621, 3423, 2924, 1631, 1448, 1426, 1387, 1032, 917, 799, 777, 748, 694, 691, 533, 468)
6	(3697, 3621, 3423, 2933, 1640, 1433, 1031, 914, 875, 781, 535, 467)
7	(3697, 3621, 3427, 2922, 1645, 1630, 1423, 1032, 913, 786, 761, 740, 694, 690, 663, 637, 536, 467, 436)
8	(3696, 3620, 3425, 2927, 1639, 1411, 1384, 1030, 914, 780, 535, 467)
9	(3696, 3620, 3425, 2925, 2854, 1640, 1440, 1385, 1098, 1030, 912, 876, 793, 765, 693, 690, 537, 466, 433)
10	(3696, 3620, 3422, 2925, 2855, 1798, 1640, 1430, 1386, 1031, 914, 875, 785, 693, 535, 467)
11	(3697, 3621, 3422, 2959, 2925, 2856, 1639, 1432, 1387, 1032, 914, 875, 784, 693, 534, 467)
Clay (<2 $\mu\text{m}$ )	
1	(3697, 3621, 3427, 2966, 2809, 1780, 1742, 1644, 1566, 1532, 1465, 1434, 1406, 1378, 1342, 1031, 913, 799, 780, 750, 692, 659, 534, 467)
2	(3697, 3621, 3423, 2932, 2857, 1640, 1385, 1031, 913, 797, 753, 693, 535, 467, 432)
3	(3697, 3621, 3423, 2928, 2854, 1724, 1639, 1449, 1386, 1032, 913, 875, 795, 756, 695, 533, 467, 430)
4	(3697, 3621, 3426, 2936, 2857, 1642, 1427, 1387, 1032, 913, 797, 753, 695, 534, 467)
5	(3697, 3621, 3424, 2925, 2854, 1640, 1438, 1384, 1032, 913, 797, 753, 695, 534, 467)
6	(3697, 3621, 3423, 2512, 1800, 1642, 1447, 1031, 913, 875, 797, 753, 694, 534, 467, 432)
7	(3697, 3622, 3425, 2927, 2855, 1640, 1429, 1385, 1032, 913, 797, 753, 694, 534, 467, 433)
8	(3697, 3622, 3425, 1640, 1407, 1385, 1032, 913, 797, 782, 753, 694, 534, 467, 430)
9	(3697, 3621, 3426, 2965, 2925, 2856, 1640, 1435, 1387, 1032, 913, 876, 797, 782, 754, 694, 534, 467, 433)
10	(3696, 3621, 3423, 2927, 2855, 1797, 1640, 1448, 1031, 913, 875, 797, 754, 694, 533, 467)
11	(3696, 3621, 3423, 2927, 2855, 2516, 1798, 1640, 1440, 1031, 913, 875, 797, 754, 694, 533, 467)

### 3.7.1 FTIR spectra bands related to clay minerals presence

Results of IR spectra of the investigated silt and clay fractions were illustrated in Fig. 4 and Table 5. The bands at 3615 to 3622  $\text{cm}^{-1}$  and 911 to 918  $\text{cm}^{-1}$  represent the dioctahedral smectites (Tomić et al. 2011) which come from stretching ( $\nu$ ) and deformation ( $\delta$ ) vibrations, respectively, of hydroxyls in the [Al–Al–OH] structure (Frost et al. 2002). According to Khang et al. (2016), Smectite (montmorillonite) minerals' IR spectra are identified in the studied fractions by a double absorption peak around 3620  $\text{cm}^{-1}$  and 3400  $\text{cm}^{-1}$ , a strong peak at 1032  $\text{cm}^{-1}$  (Fig. 4 and Table 5). The bands at 3621, 3421, 912, 799, and 750  $\text{cm}^{-1}$  were assigned to the illite mineral (Owino 2016). In the IR spectra, the structure of pure Kaolinite exhibits four well-defined (-OH) bands, three of them (3652, 3671, and 3694  $\text{cm}^{-1}$ ) describe the stretching vibrations of surface hydroxyl groups, whereas the fourth (3620  $\text{cm}^{-1}$ ) is associated with the vibrations of inner OH groups (Djomgoue and Njopwouo 2013; Gates et al. 2017; Ritz et al. 2011), the studied silt and clay fractions samples showed bands at 3620 and 3697  $\text{cm}^{-1}$ . Al–O–H in Kaolinite appears at bands 3694–3697 and 3625–3617  $\text{cm}^{-1}$ , and H–O–H of Kaolinite or montmorillonite appears at bands 3423  $\text{cm}^{-1}$  (Lugwisha 2011). In the studied fractions, montmorillonite appears at band 3423  $\text{cm}^{-1}$  (El-Habaak et al. 2018). The shoulder at 3695  $\text{cm}^{-1}$  and the weak band at 694  $\text{cm}^{-1}$  in the samples propose that kaolinite is present (Lugwisha 2011). The absorption bands between 3420 and 3445  $\text{cm}^{-1}$  may be assigned to the OH vibrational mode of the hydroxyl molecule in most of natural hydrous silicates (Saikia and Parthasarathy 2010).

### 3.7.2 FTIR spectra bands related to non-clay minerals presence

The non-clay minerals in the investigated silt and clay fractions were recorded in the FTIR spectra (Fig. 4 and Table 5). The bands at 799–795  $\text{cm}^{-1}$  and 777–779  $\text{cm}^{-1}$ , 754 and 690–695  $\text{cm}^{-1}$  are characteristic of quartz (Russell 1987; Saikia and Parthasarathy 2010; Sathya et al. 2012). Carbonate minerals represented by calcite appeared at the bands 1427 to 1433 (Kim et al. 2021) and 875 to 870  $\text{cm}^{-1}$  (Bosch Reig et al. 2002; Ravisankar et al. 2010). Feldspar appeared at the bands 1090, 1030, 1032, 533, and 466  $\text{cm}^{-1}$  (Jozanikohan and Abarghooei 2022). The bands between 1620 and 1642  $\text{cm}^{-1}$  are attributed to H–O–H (water) bending vibrations (Saikia and Parthasarathy 2010; Sergeeva et al. 2019). The band centered at 1636  $\text{cm}^{-1}$  was due to the deformation mode of physically adsorbed water molecules. This band was wide; therefore, it most likely overlapped bands at 1680 and 1650  $\text{cm}^{-1}$ , corresponding to water deformation modes consistent with the interlayer cations and water in their hydration sphere, respectively (Frost et al. 2002).

### 3.7.3 FTIR spectra bands related to organic matter presence

It was noted that some bands do not belong to any of the clay- or non-clay minerals, which may be due to the presence of organic matter (Fig. 4 and Table 5). The bands at 2970, 2941  $\text{cm}^{-1}$ , and 2885  $\text{cm}^{-1}$  ascribed to the Methyl C–H stretch. Ali et al. (2018) indicated that the peaks at 2935 and 2893  $\text{cm}^{-1}$  belong to the O–H and C–H stretching vibrations of carboxylic acid, alcohol, or alkene groups. The centred bands at 2925, and 2854  $\text{cm}^{-1}$ , correspond to asymmetric stretching vibrations of  $\text{CH}_3$  and  $\text{CH}_2$  groups, respectively (Karthek and David 2018). The C=O group showed absorption bands at 2511–2516  $\text{cm}^{-1}$  (Pereira et al. 2017). Based on Piqueras et al. (2020), the C=O stretch vibration of acetyl or carboxylic acid (COOH) groups is thought to provide distinct broadband in the IR spectra at 1700–1736  $\text{cm}^{-1}$ . A peak around 1745  $\text{cm}^{-1}$  and bands at 1790–1775  $\text{cm}^{-1}$  defines the carbonyl (C=O) group stretching (Samargandi et al. 2014; Volkov et al. 2021). Onyiriuka (1996) and Mohd-Rus et al. (2009) showed that the peaks at 1720–1740  $\text{cm}^{-1}$  are assumed to be formed by aliphatic aldehydes. Ali et al. (2018) found that a very definite peak at 1662  $\text{cm}^{-1}$ , which then shifted to 1639  $\text{cm}^{-1}$ , indicated the C=O or C=C stretching vibration of acid derivatives presence. Also, the carboxylic (-COOH) group gives a peak at 1633  $\text{cm}^{-1}$ . Regarding the typical spectra charts, the peaks at 1640–1690  $\text{cm}^{-1}$  may be formed by C=O stretching (Piqueras et al. 2020). Furthermore, bending that appears at 1643 and 1639  $\text{cm}^{-1}$  is related to the stretching of C=O groups (Syu and Prendergast 1997; Huang et al. 2018). Bands at 1532 and 1566  $\text{cm}^{-1}$  related to COO- stretching (Rumpel et al. 2001), Peaks at 1485–1445  $\text{cm}^{-1}$  refer to Methylene C–H (Coates 2000; Nandiyanto et al. 2019). Peaks at 1378  $\text{cm}^{-1}$  defined the  $\text{CH}_3$  group (symmetrical deformation) (Pereira 2017). The aliphatic C–H stretching peaks at 1380–1387  $\text{cm}^{-1}$  (Samargandi et al. 2014). While peaks at 1390–1380  $\text{cm}^{-1}$  represent a symmetric stretch carboxylate (Volkov et al. 2021).

## 4 Discussion

Soil physiochemical properties are interrelated and affected by land use and management activities. Based on soil physiochemical properties determination, the results indicated that the studied soils were slightly alkaline, which may be related to less leaching of basic cations from these soils (Selmy et al. 2022). According to  $\text{EC}_e$  values and Richards (1954) criteria, the very slight or slight salinity in all the investigated soil samples may be due to the quality of Nile irrigation water, which can remove the soluble salts from the root zone in the Nile Valley soils, and the sufficient natural

drainage of these soils. Similar results were reported by Ragheb et al. (2017) and Abuzaid (2018). The total calcium carbonate (%) results did not show strong differences among the studied soils. That could be because  $\text{CaCO}_3$  is less mobile compared to other salts, i.e., it only moves as  $\text{Ca}(\text{HCO}_3)_2$  solution salts to be precipitated again when the water has evaporated. These results agreed with the findings of Sulieman et al. (2016) in the River Nile terrace soils, Assiut Governorate, Egypt. According to Hazelton and Murphy (2016), the examined soil samples had a high cation exchange capacity (CEC), which may be due to their fine texture, high content of fine particles (% silt + % clay), and organic matter. Similar results were obtained by Abuzaid (2018) and Abowaly et al. (2023).

Soil organic carbon content (% OC) of the investigated soil samples is moderate to high (Hazelton and Murphy 2016), which could be attributed to the agricultural practices, the long age of cultivation, and the presence of clay particles which form a resistant clay-humus complex (Selmy et al. 2022). A positive and significant ( $R^2=0.8500^{**}$ ) linear relationship between OC content ( $\text{g OC kg}^{-1}$  soil) in the studied bulk soil samples and fine particles (silt + clay) percentage in these samples was recorded. The total nitrogen content (% TN) of the examined soil samples correlated with their organic matter content and agriculture activities. According to the regression equations and  $R^2$  values (Table 6), there was a positive and significant ( $R^2=0.7816^{**}$ ) linear relationship between soil total N content ( $\text{g N kg}^{-1}$  soil) and the fine particles (silt + clay) percentage in soil samples. These results agree with the finding reported by Spohn and Stendahl (2022) about the organic C and N contents in fine-textured soils compared with coarse-textured soils.

Fine fractions characteristics may have an important effect on the soil's physicochemical reactions and properties. The CEC values of the fine fractions (silt and clay) increased with particle size decrease. According to the results of cation exchange capacity (CEC), it is evident that the fine fractions,

especially clay, have the major portion in soil CEC, which may be related to the high phyllosilicates content of clay fractions compared to silt ones. Phyllosilicate minerals are characterized by their platy structure. They are composed of two types of horizontal sheets; one is dominated by silicon (silica tetrahedral sheet) and the other by aluminum and/or magnesium (alumina octahedral sheet). In the tetrahedral sheets, the  $\text{Si}^{4+}$  ions can be substituted by  $\text{Al}^{3+}$  ions; in the octahedral sheets, the  $\text{Al}^{3+}$  can be substituted by  $\text{Mg}^{2+}$ . This process is called "isomorphic substitution," which results in net permanent negative charges in the clay layer. These negative charges may be compensated by the adsorption of positive cations on phyllosilicate layer surfaces, thus increasing the CEC. Similar results were obtained by Van Der Kellen et al. (2022). Moreover, the high SSA values of clay fractions in comparison with silt fractions could also be attributed to their higher content of phyllosilicates. These results are in agreement with Castellano et al. (2015) and Schweizer et al. (2021).

Based on the results of Pearson correlation coefficient (Table 7), this study showed that the CEC of the assessed fine fractions positively significantly correlated with SSA and phyllosilicates content ( $r=0.823^{**}$  and  $0.851^{**}$ , respectively) (Singh et al. 2018; Xue et al. 2022) and negatively significant correlated with non-phyllosilicate minerals (feldspars, calcite, and quartz) content of the fine fractions ( $r=-0.761^{**}$ ,  $-0.512^*$  and  $-0.890^{**}$ , respectively). A highly significant positive correlation was observed between the fine fraction's SSA values and phyllosilicates content ( $r=0.856^{**}$ ), while the SSA negatively significantly correlated with feldspars, calcite, and quartz contents of the fine fraction ( $r=-0.788^{**}$ ,  $-0.510^*$  and  $-0.875^{**}$ , respectively). These findings matched with the results of Das et al. (2022) and Yin et al. (2023).

Fine fractions-associated OC is considered one of the stable carbon pools in the soil. Results indicated that the organic carbon content in clay fractions of all studied soils

**Table 6** The linear regression relationships

Bulk soil
OC content ( $\text{g kg}^{-1}$ ) in bulk soil = $0.1005(\text{silt} + \text{clay} \%) + 9.688$ ( $R^2=0.8500^{**}$ , $\text{SE} = \pm 0.831$ )
Total N content ( $\text{g kg}^{-1}$ ) in bulk soil = $0.0145(\text{silt} + \text{clay} \%) + 1.1125$ ( $R^2=0.7816^{**}$ , $\text{SE} = \pm 0.151$ )
Silt (63–2 $\mu\text{m}$ ) fraction
OC-silt ( $\text{g kg}^{-1}$ soil) = $0.1544(\text{silt} \% \text{ in bulk soil}) + 0.8223$ ( $R^2=0.8169^{**}$ , $\text{SE} = \pm 0.945$ )
Total N-silt ( $\text{g kg}^{-1}$ soil) = $0.0178(\text{silt} \% \text{ in bulk soil}) + 0.1286$ ( $R^2=0.7974^{**}$ , $\text{SE} = \pm 0.116$ )
Clay (<2 $\mu\text{m}$ ) fraction
OC-clay ( $\text{g kg}^{-1}$ soil) = $0.1547(\text{clay} \% \text{ in bulk soil}) + 2.5238$ ( $R^2=0.8830^{**}$ , $\text{SE} = \pm 0.899$ )
Total N-clay ( $\text{g kg}^{-1}$ soil) = $0.019(\text{clay} \% \text{ in bulk soil}) + 0.3671$ ( $R^2=0.8295^{**}$ , $\text{SE} = \pm 0.137$ )
OC-silt and Total N-silt = organic C and total N associated with silt fraction
OC-clay and Total N-clay = organic C and total N associated with clay fraction
$R^2$ = Coefficient of determination., SE = standard error of the estimate
** The p values of slope were highly significant ( $p < 0.001$ )

**Table 7** Pearson's correlation coefficient between fine fractions characteristics

	CEC	SSA	OC	TN	Phyllo (%)	Feldsp. (%)	Calc. (%)	Qua. (%)
CEC								
SSA	0.823**							
OC	0.682**	0.421 ns						
TN	0.687**	0.429*	0.940**					
Phyllo. (%)	0.851**	0.856**	0.543**	0.586**				
Feldsp. (%)	-0.761**	-0.788**	-0.499*	-0.571**	-0.970**			
Calc. (%)	-0.512*	-0.510*	-0.383 ns	-0.294 ns	-0.535*	0.412 ns		
Qua. (%)	-0.890**	-0.875**	-0.531*	-0.544**	-0.926**	0.817**	0.513*	

CEC = cation exchange capacity of fraction (cmol(+) kg<sup>-1</sup>), SSA = specific surface area (m<sup>2</sup> g<sup>-1</sup>)

OC and TN = organic C (g OC kg<sup>-1</sup> fraction) and total nitrogen (g TN kg<sup>-1</sup> fraction) contents

Phyllo. = Phyllosilicates; Feldsp. = Feldspars; Calc. = Calcite; Qua. = Quartz

ns = the correlation is not significant

\* Correlation is significant at the 0.05 level

\*\* Correlation is significant at the 0.01 level

is greater than in the silt fractions. A similar trend was observed by Covalada et al. (2007), who reported that 60, 30, and 1% of the total soil organic carbon in Acrisols was associated with clay, silt, and sand fractions, respectively. Regarding the linear relationships, there was a positive and significant ( $R^2 = 0.8169^{**}$ ) linear relationship between OC associated with silt fraction (g OC kg<sup>-1</sup> soil) and the silt fraction percentage in bulk soil. Also, there was a positive and significant ( $R^2 = 0.8830^{**}$ ) linear relationship between OC associated with clay fraction (g OC kg<sup>-1</sup> soil) and the clay fraction percentage in the bulk soil. Therefore it seems that the soil's capacity to store or protect OC correlates with the amount of fine particles. Yang et al. (2016) noticed that 70–98% of bulk soil's OC was associated with silt + clay size fraction.

Pearson correlation coefficient results showed that the organic carbon (OC) content of the fine fractions (silt and clay) samples had a highly significant positive correlation with CEC and phyllosilicates content (%) of the fine fraction with *r* values of 0.682\*\* and 0.543\*\*, respectively. The high CEC promotes the adsorption of the organic compound onto the phyllosilicate surfaces by cation bridging, van der Waals interactions, hydrogen bonding, and ligand exchange interactions and encourages the organo-mineral assemblages (Barré et al. 2014; Hu et al. 2021). Furthermore, there were significant negative correlations between the organic C content of fine fractions and the percentages of feldspars minerals and quartz in these fractions ( $r = -0.499^*$  and  $-0.531^*$ , respectively), which may be due to the very low surface charges, exchange sites and SSA of these minerals.

According to the linear regression relationships, the relationship between total N associated with each fine fraction (g N kg<sup>-1</sup> soil) and the percentage of that fraction in the bulk soil was positive and significant ( $R^2 = 0.7974^{**}$  and

0.8295\*\* for silt and clay, respectively). These results indicate that the soil N content is jointly affected by the presence of fine particles (Lu et al. 2023). The total N content aligned with the trend of organic C content in all the examined fine fractions. According to Pearson correlation coefficient, the total N content values of the fine fractions showed significant positive correlations with CEC, SSA, phyllosilicates, and organic carbon contents of these fractions ( $r = 0.687^{**}$ ,  $-0.429^*$ ,  $0.586^{**}$ , and  $0.940^{**}$ , respectively), and significantly negative ones with the fine fractions contents of feldspars and quartz with *r* values of  $-0.571^{**}$  and  $-0.544^{**}$ , respectively. This similarity confirms that most soil N reserves are organic, and the N and C cycles are coupled tightly (Lu et al. 2021). Because no N-bearing minerals are found in soil, the only nitrogen source is the organic matter applied to the soil through cultivation activities. Stabilizing organic matter in soil improves the N supply for plants.

The content and composition of clay minerals in soils greatly affect the restriction of SOC mineralization. As regards the clay mineral species of clay fractions, it can be noticed that the rich-smectite (smectite/illite mixed-layers) mineral is dominant in the clay fractions of the studied soils, which may explain the higher OC-associated with clay fractions compared to silt ones in the studied fruit orchards soils. The greater ability of smectites and mixed-layer illite/smectite to protect organic matter (OM) may be related to the presence of Ca<sup>2+</sup>, as interstratified in the structure of smectite and rich-smectite (smectite/illite mixed-layers) mineral ( $S/I_{sm}$ ) which encourages the binding between the negatively charged surfaces of clay minerals and the negatively charged or polarized organic molecules via cation bridging. Similar results were stated by Rowley et al. (2018) and Lutfalla et al. (2019). The high CEC of 2:1 clay minerals like smectite enhances the organo-mineral interaction between

the organic C and this type of minerals and increases the adsorption of the organic molecules on the surfaces of these minerals (Matus et al. 2016; Sarkar et al. 2018). The specific surface area of smectite > illite > kaolinite (Singh et al. 2018). Smectite and rich-smectite (smectite/illite mixed-layers) minerals could absorb more OM since they have a high specific surface area (Lutfalla et al. 2019; Schweizer et al. 2019). Moreover, since the smectites are expanded minerals, the organic cations and molecules can be adsorbed on these minerals' charged external and internal surfaces (Churchman et al. 2020). These factors can explain the assessed clay fractions' higher organic C and N contents. Unlike smectites,  $K^+$  ions compensate most of the negative charges of illite surfaces;  $K^+$  ions are less effective as bridges between mineral surfaces and organic molecules because they are monovalent, have a lower charge: radius ratio, and have a lower charge (Lutfalla et al. 2019). The investigated clay fractions contained a significant amount of kaolinite and kaolinite/ smectite mixed layers minerals which encouraged the organic carbon association with clay particles. This is in line with Wang et al. (2018) who reported a direct correlation between the aromaticity of humic substances and their adsorption affinity onto kaolin clay. The capacity of clay minerals to stabilize the organic C follows the order of Smectite > illite > kaolinite (Hu et al. 2021). Saidy et al. (2012) studied the effect of clay mineralogy on the mineralization rate of organic carbon and observed that this rate was lower in the presence of the illitic or smectitic clays than in kaolinitic clays. Ngole and Ekosse (2009) found similar results in Vertisols dominated by smectitic mineral clay compared to soils dominated by Kaolinite, feldspars, and quartz. El-sayed et al. (2019) found that montmorillonite prefers to adsorb the aliphatic fractions of humic acid. Ghosh et al. (2009) also observed a tendency of peat humic acid's polymethylene groups to adsorb on kaolinite, whereas more aromatic compounds were adsorbed on montmorillonite. Also, Zhang et al. (2012) suggested that on Kaolinite and Smectite, more humic acid was adsorbed than fulvic acid, but more fulvic acid than humic acid was adsorbed onto vermiculite. Thus, the dominant clay mineral species greatly affect the formation of organo-mineral complexes in the soil.

## 5 Conclusion

The studies on the organic carbon storage potential of Nile floodplain soils in Egypt are essential for obtaining baseline information on the existing soil organic carbon (SOC) stocks, as these soils represent the major part of Egypt's agricultural land area. The soils of old cultivated fruit orchards in the Nile floodplains of Sohag, Egypt were chosen for this study because, as would be expected, they have a significant level of organic matter. This study assumed that the

characteristics and mineralogy of soil fine mineral particles can affect the organic C and N sequestration in soil. A variation in the organic matter content in the investigated soils was found, and the majority of soil organic carbon (about 89%, as mean) was associated with silt and clay-sized particles. Silt and clay fractions stored about 87% (as mean) of the soil's total nitrogen content. The results confirmed that the fine fraction content of organic C and N highly significantly correlated with their physiochemical characteristics and mineralogical composition. The organic matter association with fine particles (clay and silt) is considered one of the essential aspects in its physical protection against biological and chemical decomposition in the soil and thus improving soil health and sustainability. Therefore, considering the insufficient knowledge and few studies, we recommend doing more studies on the impact of soil fractions and soil clay minerals on organic carbon (OC) sequestration and the OC pools turnover in Nile floodplains soils of Egypt.

**Supplementary Information** The online version contains supplementary material available at <https://doi.org/10.1007/s42729-023-01209-3>.

**Funding** Open access funding provided by The Science, Technology & Innovation Funding Authority (STDF) in cooperation with The Egyptian Knowledge Bank (EKB). The authors did not receive support from any organization for the submitted work.

**Data Availability** The data that support the finding of this study are available from the corresponding author upon reasonable request.

## Declarations

**Conflict of Interest** The authors declare that they have no competing interests relevant to the content of this article.

**Open Access** This article is licensed under a Creative Commons Attribution 4.0 International License, which permits use, sharing, adaptation, distribution and reproduction in any medium or format, as long as you give appropriate credit to the original author(s) and the source, provide a link to the Creative Commons licence, and indicate if changes were made. The images or other third party material in this article are included in the article's Creative Commons licence, unless indicated otherwise in a credit line to the material. If material is not included in the article's Creative Commons licence and your intended use is not permitted by statutory regulation or exceeds the permitted use, you will need to obtain permission directly from the copyright holder. To view a copy of this licence, visit <http://creativecommons.org/licenses/by/4.0/>.

## References

- Abowaly ME, Ali RA, Moghanm FS, Gharib MS, Moustapha ME, Elbagory M, Omara A, Elmahdy SM (2022) Assessment of Soil Degradation and Hazards of Some Heavy Metals, Using Remote Sensing and GIS Techniques in the Northern Part of the Nile Delta Egypt. *Agriculture* 13(1):76. <https://doi.org/10.3390/agriculture13010076>
- Abu Seif ES (2015) Geological evolution of Nile Valley, west Sohag, Upper Egypt: a geotechnical perception. *Arab J Geosci* 8:11049–11072. <https://doi.org/10.1007/s12517-015-1966-5>



- Abu Seif ES, El-Shater AA (2010) Engineering aspects and associated problems of floodplain deposits in Sohag Governorate, Upper Egypt. *Journal of American Science* 6:1614–1623. <http://www.americanscience.org>
- Abu Seif ES, El-Shater AA, Amin A (2022) Geological evolution and swelling potentiality of Paleo-nile Clays in Nile Valley, east Sohag, Upper Egypt. *Sohag J Sci* 7:11–28. <https://doi.org/10.21608/sjsoci.2022.249078>
- Abuzaid AS (2018) Assessing degradation of floodplain soils in north east Nile Delta, Egypt. *Egyptian Journal of Soil Science* 58(2): 135–146. <https://doi.org/10.21608/ejss.2017.1717.1130>
- Al-Farraj AS (2008) The mineralogy of clay fractions in the soils of the southern region of Jazan Saudi Arabia. *J Agron* 7:115–126
- Ali I, Peng C, Yea T, Naz I (2018) Sorption of cationic malachite green dye on phyto-genetic magnetic nanoparticles functionalized by 3-marcaptopropanic acid. *RSC Adv* 8:8878–8897. <https://doi.org/10.1039/c8ra00245b>
- Baldock JA, Broos K (2011) Soil organic matter. In P. M. Huang, Y. Li, & M. E. Sumner (Eds.), *Handbook of soil sciences: resource management and environmental impacts* (2<sup>nd</sup> ed., pp. 1-52). Boca Raton: CRC Press
- Baldock JA, Skjemstad JO (2000) Role of the soil matrix and minerals in protecting natural organic materials against biological attack. *Org Geochem* 31:697–710. [https://doi.org/10.1016/S0146-6380\(00\)00049-8](https://doi.org/10.1016/S0146-6380(00)00049-8)
- Barré P, Velde B, Catel N, Abbadié L (2007) Soil-plant potassium transfer: impact of plant activity on clay minerals as seen from X-ray diffraction. *Plant Soil* 292(1):137–146. <https://doi.org/10.1007/s11104-007-9208-6>
- Barré P, Fernandez-Ugalde O, Virto I, Velde B, Chenu C (2014) Impact of phyllosilicate mineralogy on organic carbon stabilization in soils: incomplete knowledge and exciting prospects. *Geoderma* 235–236:382–395. <https://doi.org/10.1016/j.geoderma.2014.07.029>
- Baruah TC, Barthakur HPA (1997) *Textbook of soil analysis*. Vikas Publishing House PVT LTD, New Delhi, India
- Blanco-Canqui H, Shapiro ChA, Wortmann ChS, Drijber RA, Mamo M, Shaver TM, Ferguson RB (2013) Soil organic carbon: The value to soil properties. *J Soil Water Conserv* 68:129A-134A. <https://doi.org/10.2489/jswc.68.5.129A>
- Bock MJ, Mayer LM (2000) Mesodensity organo-clay associations in a near-shore sediment. *Mar Geol* 163:65–75. [https://doi.org/10.1016/S0025-3227\(99\)00105-x](https://doi.org/10.1016/S0025-3227(99)00105-x)
- Bosch Reig F, Gimeno Adelantado JV, Moya Moreno MC (2002) FTIR Quantitative Analysis of calcium carbonate (calcite) and silica (quartz) mixtures using the constant ratio method. Application to geological samples. *Talanta* 58:811–821. [https://doi.org/10.1016/S0039-9140\(02\)00372-7](https://doi.org/10.1016/S0039-9140(02)00372-7)
- Brindley GW (1981) X-ray identification (with ancillary techniques) of clay minerals. In: Longstaffe FJ (ed) *Short course in clays and the Resource Geologist*. Mineralogical Association of Canada, pp. 22–35.
- Brunauer S, Emmett PH, Teller E (1938) Absorption of gases in multimolecular layers. *J Am Chem Soc* 60:309–319. <https://doi.org/10.1021/ja01269a023>
- Castellano MJ, Mueller KE, Olk DC, Sawyer JE, Six J (2015) Integrating plant litter quality, soil organic matter stabilization, and the carbon saturation concept. *Global Change Biol* 21:3200–3209. <https://doi.org/10.1111/gcb.12982>
- Churchman GJ, Singh M, Schapel A, Sarkar B, Bolan N (2020) Clay minerals as the key to the sequestration of carbon in soils. *Clays Clay Miner* 68:135–143. <https://doi.org/10.1007/s42860-020-00071-z>
- Coates J (2000) Interpretation of infrared spectra, a practical approach. In: *Encyclopedia of Analytical Chemistry* R.A. Meyers (Ed.), John Wiley & Sons Ltd. Chichester 12:10881–10882
- Covalea S, Gallardo JF, Garcia-Oliva F, Christian P, Bravo M, Kirchmann H (2007) Carbon distribution on soil particle-size fractions along an altitudinal gradient in the trans-mexican volcanic belt. *International Symposium on Organic Matter Dynamics in Agro-Ecosystems*, Poitiers (FRA), 16–19/07/2007
- Das A, Purakayastha TJ, Ahmed N, Das R, Biswas S, Shivay YS, Sehgal VK, Rani K, Trivedi A, Tigga P, Sahoo J, Chakraborty R, Sen S (2022) Influence of Clay Mineralogy on Soil Organic Carbon Stabilization under Tropical Climate, India. *Journal of Soil Science and Plant Nutrition*:1–16. <https://doi.org/10.1007/s42729-022-01099-x>
- Dhaliwal SS, Naresh RK, Gupta RK, Panwar AS, Mahajan NC, Singh R, Mandal A (2020) Effect of tillage and straw return on carbon footprints, soil organic carbon fractions and soil microbial community in different textured soils under rice–wheat rotation: a review. *Rev Environ Sci Biotechnol* 19(1):103–115. <https://doi.org/10.1007/s11157-019-09520-1>
- Djomgoue P, Njopwouo D (2013) FT-IR Spectroscopy Applied for Surface Clays Characterization. *J Surf Eng Mater Adv Technol* 3:275–282. <https://doi.org/10.4236/jsemat.2013.34037>
- El-Habaak G, Askalany M, Abdel-Hakeem M (2018) The effect of mineralogy of calcined shales on the alkali activation and geopolymerization reactions: A case study from Abu-Tartur plateau, Western Desert Egypt. *Appl Clay Sci* 162:90–100. <https://doi.org/10.1016/j.clay.2018.05.025>
- El-sayed ME, Khalaf MM, Gibson D, Rice JA (2019) Assessment of clay mineral selectivity for adsorption of aliphatic/aromatic humic acid fraction. *Chem Geol* 511:21–27. <https://doi.org/10.1016/j.chemgeo.2019.02.034>
- El-Shater A, Mahran TM, Abu Seif ES, Mahmoud K (2020) Geotechnical study on the utilization of Pleistocene Sands in Sohag Basin (Upper Egypt) as a construction raw material. *Environ Earth Sci* 79:534. <https://doi.org/10.1007/s12665-020-09302-x>
- El-Shater A (2013) Characterization of soil clay minerals of the River Nile sediments, Sohag region, Egypt. Decomposition of X-ray diffraction patterns. *J Earth Sci Eng* 1:1–13
- ESRI (2016) Arc Map version 10.4.1 User Manual. ESRI, 380 New York Street, Redlands, California, 92373–8100, USA.
- Faragallah MA, Essa MA (2006) Alteration of some alluvial soils irrigated with different water resources, Assiut Egypt. *Assiut J Agric Sci* 37:165–184
- Farmer VC (1974) *The infrared spectra of minerals*. Mineralogical Society, London <https://doi.org/10.1180/mono-4>
- Feng W, Plante AF, Six J (2013) Improving estimates of maximal organic carbon stabilization by fine soil particles. *Biogeochemistry* 112:81–93. <https://doi.org/10.1007/s10533-011-9679-7>
- Feng XJ, Simpson AJ, Simpson MJ (2006) Investigating the role of mineral-bound humic acid in phenanthrene sorption. *Environ Sci Technol* 40:3260–3266. <https://doi.org/10.1021/es0521472>
- Frost RL, Klopogge JT, Ding A (2002) Near-infrared spectroscopic study of nontronites and ferruginous Smectite. *Spectrochimica Acta Part A* 58(8):1657–1668. [https://doi.org/10.1016/S1386-1425\(01\)00637-0](https://doi.org/10.1016/S1386-1425(01)00637-0)
- Gates W, Klopogge JT, Madejova J, Bergaya, F (2017) Infrared and Raman spectroscopies of clay minerals. Volume 8 (1st ed.) in the *Developments in Clay Science series*. Elsevier Ltd
- Gee GW, Bauder JW (1994) Particle-size Analysis. In: *Methods of Soil Analysis*. Part 1, 2<sup>nd</sup>. Physical and Mineralogical Methods, Klute, A. (Ed.). SSSA and ASA, Madison, WI., USA, pp. 377–382
- Ghazala HH, Ibraheem IM, Haggag M, Lamees M (2018) An integrated approach to evaluate the possibility of urban development around Sohag Governorate, Egypt, using potential field data. *Arab J Geosci* 11:194. <https://doi.org/10.1007/s12517-018-3535-1>
- Ghosh S, Zhen-Yu WANG, Kang S, Bhowmik PC, Xing BS (2009) Sorption and fractionation of a peat derived humic acid by

- kaolinite, montmorillonite, and goethite. *Pedosphere* 19(1):21–30. [https://doi.org/10.1016/S1002-0160\(08\)60080-6](https://doi.org/10.1016/S1002-0160(08)60080-6)
- Guillaume T, Makowski D, Libohova Z, Bragazza L, Sallaku F, Sinaj S (2022) Soil organic carbon saturation in cropland-grassland systems: Storage potential and soil quality. *Geoderma* 406: 115529. <https://doi.org/10.1016/j.geoderma.2021.115529>
- Guo J, Wang B, Wang G, Myo STZ, Cao F (2020) Effects of three cropland afforestation practices on the vertical distribution of soil organic carbon pools and nutrients in eastern China. *Glob Ecol Conserv* 22: e00913. <https://doi.org/10.1016/j.gecco.2020.e00913>
- Gurmu G (2019) Soil organic matter and its role in soil health and crop productivity improvement. *For Ecol Manage* 7(7):475–483
- Hassink J (1997) The capacity of soils to preserve organic C and N by their association with clay and silt particles. *Plant Soil* 191:77–87. <https://doi.org/10.1023/A:1004213929699>
- Hassink J, Whitmore APA (1997) A model of the physical protection of organic matter in soils. *Soil Sci Soc Am J* 61:131–139. <https://doi.org/10.2136/sssaj1997.03615995006100010020x>
- Hazelton P, Murphy B (2016) Interpreting soil test results: what do all the numbers mean? CSIRO publishing, Collingwood Victoria, Australia
- Heckman K, Lawrence CR, Harden JW (2018) A sequential selective dissolution method to quantify storage and stability of organic carbon associated with Al and Fe hydroxide phases. *Geoderma* 312:24–35. <https://doi.org/10.1016/j.geoderma.2017.09.043>
- Heister K (2014) The measurement of the specific surface area of soils by gas and polar liquid adsorption methods - Limitations and potentials. *Geoderma* 216:75–87. <https://doi.org/10.1016/j.geoderma.2013.10.015>
- Hillier S (2003) Quantitative analysis of clay and other minerals in sandstones by X-ray powder diffraction (XRPD). In: *Clay Minerals Cements in Sandstones* (R.H. Worden and S. Morad, editors), *Assoc Sedimentol Spec Publ* 34:213–251. <https://doi.org/10.1002/9781444304336.ch11>
- Hu N, Zhao L, Li Q, Jiang Y, Sui B, Wang H (2021) Changes in carbon fractions with corn straw incorporation and comparison of carbon sequestration efficiency in Phaeozem derived from two parent materials in China. *Arab J Geosci* 14(14):1–10. <https://doi.org/10.1007/s12517-021-07587-1>
- Huang M, Li Z, Huang B, Luo N, Zhang Q, Zhai X, Zeng G (2018) Investigating binding characteristics of cadmium and copper to DOM derived from compost and rice straw using EEM-PARAFAC combined with two-dimensional FTIR correlation analyses. *J Hazard Mater* 344:539–548. <https://doi.org/10.1016/j.jhazmat.2017.10.022>
- IBM Corp. Released (2013) IBM SPSS Statistics for Windows, Version 22.0. Armonk, NY: IBM Corp.
- Jackson ML (1973) *Soil chemical analysis*. Prentice-Hall, Inc., Englewood Cliffs, NJ, USA
- Jackson, ML (1979) *Soil Chemical Analysis Advanced Course*. Madison, Wisconsin, USA
- Johnston CT (2010) Probing the nanoscale architecture of clay minerals. *Clay Miner* 45:245–279. <https://doi.org/10.1180/claymin.2010.045.3.245>
- Johnston AE, Poulton PR, Coleman K (2009) Soil organic matter: its importance in sustainable agriculture and carbon dioxide fluxes. *Adv Agron* 101:1–57. [https://doi.org/10.1016/S0065-2113\(08\)00801-8](https://doi.org/10.1016/S0065-2113(08)00801-8)
- Jozanikohan G, Abarghooei MN (2022) The Fourier transform infrared spectroscopy (FTIR) analysis for the clay mineralogy studies in a clastic reservoir. *J Petrol Explor Prod Technol* 12:2093–2106. <https://doi.org/10.1007/s13202-021-01449-y>
- Kartheek RM, David M (2018) Assessment of fipronil toxicity on wistar rats: A hepatotoxic perspective. *Toxicol Rep* 5:448–456. <https://doi.org/10.1016/j.toxrep.2018.02.019>
- Khang VC, Korovkin MV, Ananyeva LG (2016) Identification of clay minerals in reservoir rocks by FTIR spectroscopy. *IOP Conf Ser Earth Environ Sci* 43:1–5. <https://doi.org/10.1088/1755-1315/43/1/012004>
- Kim Y, Caumon M C, Barres O, Sall A, Cauzid J (2021) Identification and composition of carbonate minerals of the calcite structure by Raman and infrared spectroscopies using portable devices. *Spectrochimica Acta Part A: Molecular and Biomolecular Spectroscopy* 261: 119980. <https://doi.org/10.1016/j.saa.2021.119980>
- Kleber M, Mikutta R, Torn MS, Jahn R (2005) Poorly crystalline mineral phases protect organic matter in acid subsoil horizons. *Eur J Soil Sci* 56:717–725. <https://doi.org/10.1111/j.1365-2389.2005.00706.x>
- Komadel P (2003) Chemically modified smectites. *Clay Miner* 38:127–138. <https://doi.org/10.1180/0009855033810083>
- Kumar M, Ghosh SK, Manjaiah K (2004) Organo-mineral complexes in some Inceptisols of India: physicochemical and thermal properties. *Commun Soil Sci Plant Anal* 35:1865–1889. <https://doi.org/10.1081/LCSS-200026808>
- Kundu DK, Ladha JK (1995) Enhancing soil nitrogen use and biological nitrogen fixation in wetland rice. *Exp Agric* 31:261–278. <https://doi.org/10.1017/S0014479700025448>
- Kunze GW, Dixon JB (1994) Pretreatment for Mineralogical Analysis. In: *Methods of Soil Analysis. Physical and Mineralogical Methods. Part 1*, Klute, A. (Ed.). SSSA and ASA, Madison, Wisconsin, USA, pp. 91–100. <https://doi.org/10.2136/sssabookser5.1.2ed.c5>
- Lanson B (1997) Decomposition of experimental X-ray diffraction patterns (profile fitting): a convenient way to study clay minerals. *Clays Clay Miner* 45:132–146. <https://doi.org/10.1346/CCMN.1997.0450202>
- Lu J, Feng S, Wang S, Zhang B, Ning Z, Wang R, Chen X, Yu L, Zhao H, Lan D, Zhao X (2023) Patterns and driving mechanism of soil organic carbon, nitrogen, and phosphorus stoichiometry across northern China's desert-grassland transition zone. *Catena* 220 (A): 106695. <https://doi.org/10.1016/j.catena.2022.106695>
- Lu X, Vitousek PM, Mao Q, Gilliam FS, Luo Y, Turner BL, Zhou G, Mo J (2021) Nitrogen deposition accelerates soil carbon sequestration in tropical forests. *Proceedings of the National Academy of Sciences* 118(16) e2020790118. <https://doi.org/10.1073/pnas.2020790118>
- Lugwisha E HJ (2011) Identification of clay minerals of the eastern southern region of lake victoria by ethylene glycol and heat: X-ray diffraction and infrared spectroscopy studies. *Tanz J Sci* 37:167–178
- Lutfalla S, Barré P, Bernard S, Le Guillou C, Alléon J, Chenu C (2019) Multidecadal persistence of organic matter in soils: multiscale investigations down to the submicron scale. *Biogeosciences* 16:1401–1410. <https://doi.org/10.5194/bg-16-1401-2019>
- Madejova J (2003) FTIR techniques in clay mineral studies. *Vibrational Spectroscopy* 31(1):1–10. [https://doi.org/10.1016/S0924-2031\(02\)00065-6](https://doi.org/10.1016/S0924-2031(02)00065-6)
- Matus F, Garrido E, Hidalgo C, Paz F, Etchevers J, Merino C, Baez YA (2016) Carbon saturation in the silt and clay particles in soils with contrasting mineralogy. *Terra Latinoamericana* 34:311–319
- Mohd-Rus AZ, Kemp TJ, Clark AJ (2009) Degradation studies of polyurethanes based on vegetable oils. Part 2. Thermal degradation and materials properties. *Progress in Reaction Kinetics and Mechanism* 34(1): 1–41. DOI: <https://doi.org/10.3184/146867809X425749>.

- Moore DM, Reynolds RC (1997) X-Ray Diffraction and the Identification and Analysis of Clay Minerals. 2nd ed., Oxford University Press, New York, pp. 378
- Nandiyanto ABD, Oktiani R, Ragadhita R (2019) How to Read and Interpret FTIR Spectroscopy of Organic Material. *Journal of Science & Technology* 4: 97–118. <https://doi.org/10.17509/ijost.v4i1.15806>
- Nelson DW, Sommers LE (1996) Total Carbon, Organic Carbon and Organic Matter. In: *Methods of Soil Analysis. Part 3. Chemical Methods*, Sparks, DL (Eds.). American Society of Agronomy/Soil Science Society of America, Madison, WI. pp. 961–1010. <https://doi.org/10.2134/agronmonogr9.2.2ed.c29>
- Nelson RE (1982) Carbonate and gypsum. In A.L. Page (ed.) *Methods of soil analysis. Part 2. 2nd ed. Agron Monogr* 9:181–197. ASA and SSSA, Madison, WI.
- Ngole VM, Ekosse GE (2009) Physico-chemistry and mineralogy related to productivity of arenosol, luvisol and vertisol. *Iran J Sci Technol A Sci* 32:99–108
- Omran AA (2008) Integration of remote sensing, geophysics and GIS to evaluate groundwater potentiality—a case study in Sohag region, Egypt. The 3<sup>rd</sup> International Conference on Water Resources and Arid Environments and the 1<sup>st</sup> Arab Water Forum
- Onyiriuka EC (1996) Modification of polystyrene cell culture surfaces by grafting a thin film of starch. *J Adhes Sci Technol* 10:617–633. <https://doi.org/10.1163/156856196X00670>
- Origin (2018) OriginLab Corporation, Northampton, MA 01060, USA
- Owino OM (2016) Chemical and mineral analysis of raw and acid-treated clays from kano plains, kisumu county, Kenya. M.Sc. Thesis, chemistry Dept., The School of pure and applied sciences of Kenyatta University, Kenya
- Pan B, Tao Sh, Dawson RW, Xing BS (2010) Formation of organo-mineral complexes as affected by particle size, pH, and dry–wet cycles. *Aust J Soil Res* 48:713–719. <https://doi.org/10.1071/SR10029>
- Pereira AS, Silva MHP, Júnior ÉPL, Paula AS, Tommasini FJ (2017) Processing and characterization of PET composites reinforced with geopolymer concrete waste. *Mater Res* 20:411–420. <https://doi.org/10.1590/1980-5373-MR-2017-0734>
- Piqueras S, Füchtner S, De Oliveira RR, Gómez-Sánchez A, Jelavic S, Keplinger T, De Juan A, Thygesen LG (2020) Understanding the formation of heartwood in larch using synchrotron infrared imaging combined with multivariate analysis and atomic force microscope infrared spectroscopy. *Front Plant Sci* 10:15. <https://doi.org/10.3389/fpls.2019.01701>
- Poirier V, Basile-Doelsch I, Balesdent J, Borschneck D, Whalen JK, Angers DA (2020) Organo-mineral interactions are more important for organic matter retention in subsoil than topsoil. *Soil Systems* 4(4):1–17. <https://doi.org/10.3390/soilsystems4010004>
- Prout JM, Shepherd KD, McGrath SP, Kirk GJ, Haefele SM (2021) What is a good level of soil organic matter? An index based on organic carbon to clay ratio. *Eur J Soil Sci* 72(6):2493–2503. <https://doi.org/10.1111/ejss.13012>
- Ragheb HMA, Gomah HH, Youssef MA, Ali AMA (2017) Fertility Status and Indices of Micronutrients in Nile Valley Soils, East of the Nile River, Assiut Governorate, Egypt. *J Soil Sci* 57(2): 189–199. <https://doi.org/10.21608/ejss.2017.3829>
- Ravisankar R, Senthilkumar G, Kiruba S, Chandrasekaran A, Jebakumar PP (2010) Mineral analysis of coastal sediment samples of Tuna, Gujarat, India. *Indian Journal of Science and Technology* 3(7): 774–780. [https://www.academia.edu/download/75121268/My\\_IJST\\_Paper.pdf](https://www.academia.edu/download/75121268/My_IJST_Paper.pdf)
- Richards LA (1954) Diagnosis and Improvement of Saline Alkali Soils. Agriculture, 160, Handbook 60, US Department of Agriculture, Washington DC.
- Ritz M, Vaculíková L, Plevová E (2011) Application of infrared spectroscopy and chemometric methods to identification of selected minerals. *Acta Geodyn Geomater* 8: 47–58. <http://hdl.handle.net/10084/84629>
- Rowell DL (1994) *Soil science: Methods and applications*. Longman Group UK Ltd, London
- Rowley MC, Grand S, Verrecchia ÉP (2018) Calcium-mediated stabilisation of soil organic carbon. *Biogeochemistry* 137:27–49. <https://doi.org/10.1007/s10533-017-0410-1>
- Rowley MC, Grand S, Spangenberg JE, Verrecchia EP (2021) Evidence linking calcium to increased organo-mineral association in soils. *Biogeochemistry* 153(3):223–241. <https://doi.org/10.1007/s10533-021-00779-7>
- Roychand P, Angove M, Tisdall J (2010) Sorptive protection of organic matter in soil. 19th World Congress of Soil Science, Soil Solutions for a Changing World 2010, 1 - 6 August 2010, Brisbane, Australia. Published on DVD
- Rumpel C, Janik LJ, Skjemstad JO, Kögel-Knabner I (2001) Quantification of carbon derived from lignite in soils using mid-infrared spectroscopy and partial least squares. *Org Geochem* 32(6):831–839
- Russell JD (1987) *A hand book of determinative methods in clay mineralogy*, (ed. Wilson, M.J., Blackie and Son Ltd)
- Saidy AR, Smernik RJ, Baldock JA, Kaiser K, Sanderman J, Macdonald LM (2012) Effects of clay mineralogy and hydrous iron oxides on labile organic carbon stabilization. *Geoderma* 173–174:104–110. <https://doi.org/10.1016/j.geoderma.2011.12.030>
- Saikia BJ, Parthasarathy G (2010) Fourier transform infrared spectroscopic characterization of Kaolinite from Assam and Meghalaya, Northeastern India. *J Mod Phys* 1:206–210. <https://doi.org/10.4236/jmp.2010.14031>
- Samargandi D, Zhang X, Liu Sh, Tian Sh (2014) Fourier Transform Infrared (FT-IR) Spectroscopy for discrimination of fenugreek seeds from different producing areas. *J Chem Pharm Res* 6:19–24
- Sarkar B, Singh M, Mandal S, Churchman GJ, Bolan NS (2018) Clay minerals–Organic matter interactions in relation to carbon stabilization in soils. *The Future of Soil Carbon: It Conservation and Formation* pp. 71–86. Academic Press. <https://doi.org/10.1016/B978-0-12-811687-6.00003-1>
- SAS Institute (2002) *The SAS system for Windows*, release 9.0. SAS Institute, Cary, NC. USA
- Sathya P, Velraj G, Meyvel S (2012) Fourier transform infrared spectroscopic study of ancient brick samples from Salavankuppam Region, Tamilnadu India. *Adv Appl Sci Res* 3(2):776–779
- Schweizer SA, Bucka FB, Graf-Rosenfellner M, Kögel-Knabner I (2019) Soil microaggregate size composition and organic matter distribution as affected by clay content. *Geoderma* 355:113901. <https://doi.org/10.1016/j.geoderma.2019.113901>
- Schlüter S, Leuther F, Albrecht L, Hoeschen C, Kilian R, Surey R, Mikutta R, Kaiser K, Mueller CW, Vogel HJ (2022) Microscale carbon distribution around pores and particulate organic matter varies with soil moisture regime. *Nat Commun* 13(1):2098. <https://doi.org/10.1038/s41467-022-29605-w>
- Schweizer SA, Mueller CW, Hoeschen C, Ivanov P, Kögel-Knabner I (2021) The role of clay content and mineral surface area for soil organic carbon storage in an arable toposequence. *Biogeochemistry* 156(3):401–420. <https://doi.org/10.1007/s10533-021-00850-3>
- Selmy SA, Abd Al-Aziz SH, Ibrahim AG, Jiménez-Ballesta R (2022) Impact of Short-Term Cultivation on Some Selected Properties of Sandy Soil in an Arid Environment. *Soil Systems* 6(4):82. <https://doi.org/10.3390/soilsystems6040082>
- Sergeeva AV, Zhitova ES, Bocharov VN (2019) Infrared and Raman spectroscopy of tschermigite, (NH<sub>4</sub>) Al (SO<sub>4</sub>)<sub>2</sub> · 12H<sub>2</sub>O. *Vibrational Spectroscopy* 105: 102983. <https://doi.org/10.1016/j.vibsp.ec.2019.102983>

- Singh M, Sarkar B, Sarkar S, Churchman J, Bolan N, Mandal S, Menon M, Purakayastha TJ, Beerling DJ (2018) Stabilization of soil organic carbon as influenced by clay mineralogy. *Adv Agron* 148:33–84. <https://doi.org/10.1016/bs.agron.2017.11.001>
- Soil Survey Staff (1996) *Keys to Soil Taxonomy*. Seventh Edition., 644 pp. USDA Natural Resource Conservation Service, Washington DC
- Sparks DL (2003) *Environmental soil chemistry*, 2nd edn. Academic Press, New York, pp 94–95
- Spohn M, Stendahl J (2022) Carbon, nitrogen, and phosphorus stoichiometry of organic matter in Swedish forest soils and its relationship with climate, tree species, and soil texture. *Biogeosciences* 19(8):2171–2186. <https://doi.org/10.5194/bg-19-2171-2022>
- Suliaman MM, Ibrahim IS, Elfaki JT (2016) Genesis and classification of some soils of the River Nile terraces: a case study of Khartoum North, Sudan. *J Geosci Environ Protect* 4(3):1–16. <https://doi.org/10.4236/gep.2016.43001>
- Syu V, Prendergast FG (1997) Water (H<sub>2</sub>O and D<sub>2</sub>O) molar absorptivity in the 1000–4000 cm<sup>-1</sup> range and quantitative infrared spectroscopy of aqueous solutions. *Anal Biochem* 248:234–245. <https://doi.org/10.1006/abio.1997.2136>
- Takahashi T, Dahlgren RA (2016) Nature, properties and function of aluminum–humus complexes in volcanic soils. *Geoderma* 263:110–121. <https://doi.org/10.1016/j.geoderma.2015.08.032>
- Tomić ZP, Antić-Mladenović SB, Babić BM, Poharc-Logar VA, Đorđević AR., Cupać SB (2011) Modification of smectite structure by sulfuric acid and characteristics of the modified smectite. *Journal of Agricultural Sciences* 56(1): 25–35. <https://scindeks.ceon.rs/article.aspx?artid=1450-81091101025T>
- Udom BE, Benwari AO, Osaro ET (2015) Organic Carbon and Nitrogen Distribution in Particle-size Fractions of Soils Under Cassava, Plantain and Rubber Based Land Use. *Int J Soil Sci* 10:166–176. <https://doi.org/10.3923/ijss.2015.166.176>
- Van Der Kellen I, Derrien D, Ghanbaja J, Turpault MP (2022) Recent weathering promotes C storage inside large phyllosilicate particles in forest soil. *Geochim Cosmochim Acta* 318:328–351. <https://doi.org/10.1016/j.gca.2021.12.009>
- Velde B (1995) Composition and mineralogy of clay minerals. In: Velde B (ed) *Origin and mineralogy of clays*. Clays and the environment. Springer, Berlin, pp. 8–42.
- Volkov DS, Rogova OB, Proskurnin MA (2021) Organic Matter and Mineral Composition of Silicate Soils: FTIR Comparison Study by Photoacoustic, Diffuse Reflectance, and Attenuated Total Reflection Modalities. *Agronomy* 11:1879. <https://doi.org/10.3390/agronomy11091879>
- Wang F, He J, He B, Zhu X, Qiao X, Peng L (2018) Formation process and mechanism of humic acid-kaolin complex determined by carbamazepine sorption experiments and various characterization methods. *J Environ Sci* 69:251–260. <https://doi.org/10.1016/j.jes.2017.10.020>
- Wei L, Ge T, Zhu Z, Luo Y, Yang Y, Xiao M, Yan Z, Li Y, Wu J, Kuzyakov Y (2021) Comparing carbon and nitrogen stocks in paddy and upland soils: Accumulation, stabilization mechanisms, and environmental drivers. *Geoderma* 398: 115121. <https://doi.org/10.1016/j.geoderma.2021.115121>
- Wibowo H, Kasno A (2021) Soil organic carbon and total nitrogen dynamics in paddy soils on the Java Island, Indonesia. In *IOP Conference Series: Earth and Environmental Science* 648(1): 012192. IOP Publishing. doi:<https://doi.org/10.1088/1755-1315/648/1/012192>
- Wiesmeier M, Urbanski L, Hobley E, Lang B, von Lützow M, Marin-Spiotta E, Wesemael BV, Rabot E, Ließ M, Garcia-Franco N, Wollschläger U, Vogel H, Kögel-Knabner I (2019) Soil organic carbon storage as a key function of soils—A review of drivers and indicators at various scales. *Geoderma* 333:149–162. <https://doi.org/10.1016/j.geoderma.2018.07.026>
- Xue B, Huang L, Li X, Lu J, Gao R, Kamran M, Fahad S (2022) Effect of clay mineralogy and soil organic carbon in aggregates under straw incorporation. *Agronomy* 12(2):534. <https://doi.org/10.3390/agronomy12020534>
- Yang XM, Drury CF, Reynolds WD, Yang JY (2016) How do changes in bulk soil organic carbon content affect carbon concentrations in individual soil particle fractions? *Sci Rep* 6(1):1–7. <https://doi.org/10.1038/srep27173>
- Yin N, Geng N, Wang T, Wang H, Pan H, Yang Q, Lou Y, Zhuge Y (2023) Effect of acidification on clay minerals and surface properties of brown soil. *Sustainability* 15(1):179. <https://doi.org/10.3390/su15010179>
- Zhang L, Luo L, Zhang Sh (2012) Integrated investigations on the adsorption mechanisms of fulvic and humic acids on three clay minerals. *Colloids and Surfaces A: Physicochem. Eng Aspects* 406:84–90. <https://doi.org/10.1016/j.colsurfa.2012.05.003>

**Publisher's Note** Springer Nature remains neutral with regard to jurisdictional claims in published maps and institutional affiliations.